Ore Geology Reviews 127 (2020) 103806

Contents lists available at ScienceDirect

Ore Geology Reviews

journal homepage: www.elsevier.com/locate/oregeorev

Origin and evolution of ore-forming fluids in a tungsten mineralization system, Middle Jiangnan orogenic belt, South China: Constraints from in-situ LA-ICP-MS analyses of scheelite

Yong Zhang [a,*], Dongsheng Ma [a,b], Jian-Feng Gao [c,*]

[a] State Key Laboratory of Nuclear Resources and Environment, East China University of Technology, Nanchang 330013, China
[b] School of Earth Sciences and Engineering, Nanjing University, Nanjing 210046, China
[c] State Key Laboratory of Ore Deposit Geochemistry, Institute of Geochemistry, Chinese Academy of Sciences, Guiyang 550081, China

ARTICLE INFO

Keywords:
Ore-forming fluid evolution
Scheelite
In-situ trace element analysis
Tungsten mineralization
Dahutang tungsten deposit
South China

ABSTRACT

The Middle Jiangnan orogenic belt is a very important tungsten (W) polymetallic belt in China. There are many types of W deposits in the belt, including veinlet-disseminated and stratabound deposits, which have different origins. The veinlet-disseminated Dahutang W deposit has undergone extensive alteration, such as biotitization (potassic alteration), and greisenization. Scheelite in veinlet-disseminated W mineralization displays a zoned texture indicating at least two generations. The early generation (D1) from the Dahutang W deposit exhibits magmatic hydrothermal characteristics with comparatively high Nb, Ta, and Mo concentrations, but a low Sr concentration (44 to 95 ppm). In contrast, the scheelite samples from the Xi'an W deposit has relatively low Nb, Ta, and Mo concentrations, but a high Sr concentration (582 to 861 ppm), mainly originating from a metamorphic fluid that mixed with meteoric water. The composition of the late generation of scheelite (D2) samples from the Dahutang deposit are intermediate between the composition of scheelite (D1) and scheelite of the Xi'an depsoit. The mineral chemistry of the scheelite samples indicate that the ore-forming fluids of the Dahutang deposit were dominated by magmatic hydrothermal fluids during the early stage, and that meteoric water was added during fluid evolution. The rare earth elements (REEs) in the scheelite samples, especially the variation of the δEu ($Eu_N/((Sm_N \times Gd_N)^{0.5})$) values, record the change in oxygen fugacity. The ore-forming fluids in the early stage of the Dahutang deposit were reduced becoming oxidized during the precipitation of the D2 scheelite, whereas the ore-forming fluids of the Xi'an deposit were oxidized. An increased oxygen fugacity of the ore-forming fluids of the Dahutang deposit restricted the precipitation of wolframite and promoted the formation of scheelite. Extensive alteration resulted in the decomposition of plagioclase, thus releasing Ca and Sr for the crystallization of scheelite at the Dahutang tungsten deposit.

1. Introduction

The Middle Jiangnan orogenic belt in south China hosts many tungsten (W) deposits of different origins (Liu et al., 1982; Liu and Ma, 1987b). However, W deposits in the belt are thought to be formed by different hydrothermal systems. The giant Dahutang W deposit has total reserves of>1.31 Mt of WO_3 (Zhang et al., 2018b), which originates from Yanshanian granites. The W orebodies are mostly distributed in the contact zone between the Yanshanian porphyritic biotite granite and Neoproterozoic biotite granodiorite. The main types of mineral deposits are veinlet-disseminated (disseminated quartz veins width from 0.01 cm to 1.0 cm), quartz veins (quartz veins width > 20 cm, usually from 20 cm to 40 cm), quartz veinlet belts (quartz veins width from 1.0 cm to 20.0 cm, usually 5.0 cm to 10 cm), and crypto-explosive breccias (Xiang et al., 2013b). In contrast, the Woxi and Xi'an Au–W deposits in northwestern Hunan are stratabound deposits, which are believed to have been formed by metamorphic and recycled meteoric water (Wan, 1985; Ma and Liu, 1992; Liu et al., 1993, 2000; Ten et al., 1999; Gu et al., 2005). It is still not well understood why these different types of W deposits could form within the same belt. Furthermore, the origin and evolution of ore-forming fluids in these W mineralization systems have not been well constrained.

Scheelite is a hydrothermal mineral that can precipitate in various types of hydrothermal systems, including W–Au–Sb, Au–Sb, and W

* Corresponding authors.
E-mail addresses: zhycy2004@163.com (Y. Zhang), gaojianfeng@mail.gyig.ac.cn (J.-F. Gao).

https://doi.org/10.1016/j.oregeorev.2020.103806
Received 14 March 2020; Received in revised form 24 September 2020; Accepted 25 September 2020
Available online 1 October 2020

deposits. Scheelite can incorporate abundant trace elements, such as rare earth elements (REEs), Sr, Y, Pb, Mn, and Mo, via substitution of Ca^{2+} or W^{6+} in the crystal lattice (Raimbault et al., 1993; Ghaderi et al., 1999; Liu et al., 2007). These substitutions are controlled mainly by the composition and physicochemical nature of the associated fluids (Sylvester and Ghaderi, 1997; Brugger et al., 2000b, 2008; Peng et al., 2010; Zhang and Peng, 2012; Song et al., 2014; Li et al., 2018; Sciuba et al., 2019). In addition, europium (Eu) has multiple valence states, whereby Eu^{3+} has a partition coefficient much higher than Eu^{2+} (Brugger et al., 2000a, 2000b). Therefore, the Eu^{2+}/Eu^{3+} ratio is particularly sensitive to the pH of ore-forming fluids and can document changes in the oxidation state of the fluids (Brugger et al., 2006, 2008). Scheelite is luminescent under an electron beam, which allows the study of textural zonation and changes in trace element composition (Sciuba et al., 2019). Elements including REEs, Y, As, and Sr in scheelite have minor effects on the cathodoluminescence (CL) response (Brugger et al., 2000a; MacRae et al., 2009; Poulin, 2016; Poulin et al., 2016), whereas variations in Mo are typically visible in cathodoluminescence (CL) images (Poulin, 2016; Poulin et al., 2016). Therefore, the CL image and elemental composition of scheelite can record changes in the compositions and physicochemical conditions of ore-forming fluids during W mineralization.

The Dahutang W deposit is a typical granite-related deposit in the Middle Jiangnan orogenic belt, whereas the Xi'an W deposit is a stratabound deposit. Northwest Hunan is one of the important Au-Sb-W regions in the Middle Jiangnan orogenic belt, South China. The genesis of Xi'an W deposit has been well defined in previous studies (Ma and Liu, 1991, 1992; Niu and Ma, 1992; Shi et al., 1993; Liu et al., 1993; Peng et al., 2003; Zhang et al., 2018d).

The chemical and mineralogical character of the scheelite from the Dahutang and Xi'an tungsten deposits may give a new perspective to understand the relationship between the magmatic hydrothermal (granite-related) W-Sn deposits and the metamorphic origin hydrothermal (stratabound) Au-W deposits, and provide new insights into the ore-forming process of the Dahutang tungsten deposit. In this study, we compare the scheelite from the Xi'an deposit sourced from metamorphic fluids mixed with deep cyclic seawater to scheelite from the Dahutang deposit. We compare the mineral texture and chemistry of the scheelite samples from the two deposits to constrain the origin and evolution of W mineralization in the Middle Jiangnan orogenic belt.

2. Regional geology

The Jiangnan orogenic belt is situated on the northeastern boundary between the Cathaysia and Yangtze blocks (Fig. 1) (Shu et al., 1995; Li et al., 2009; Shu, 2012), and is one of the important polymetallic/metallogenic belts in China. The belt is divided into three sections: the Eastern, Middle and Western Jiangnan orogenic belts (Shu et al., 1993; Zhang et al., 2013; Han et al., 2016). There are several W ore fields in the Middle Jiangnan orogenic belt, including the Jiuling W polymetallic field and the Woxi–Xi'an Au–Sb–W ore field (Fig. 1).

The Jiuling W polymetallic ore field is composed of many large to extremely large W polymetallic deposits, including the Xianglushan, Dahutang, Huashandong, Penshang, Yangculing, Lianhuaxing, and Cunqian deposits (Zhang, 2018). The exposed granite in the Jiuling W polymetallic ore field is comprised of Neoproterozoic granodiorite (Zhong et al., 2005; Wang et al., 2008). The Yanshanian granite in the ore field is composed of several phases, including I-type granite (170–160 Ma) (Ding et al., 2005; Lou et al., 2005; Hu et al., 2015) and highly differentiated S-type granite (150–130 Ma) (Liu et al., 2008a; Huang and Jiang, 2014; Li et al., 2014; Zhang et al., 2016). The W polymetallic mineralization is understood to be related to S-type granite (Liu et al., 2008a; Huang and Jiang, 2014; Li et al., 2014; Zhang et al., 2016).

The Woxi–Xi'an Au–Sb–W district consists of the Woxi W–Au–Sb, Xi'an W, Zhazixi W–Sb, and Xichong W–Sb deposits. The host rock of these deposits is metamorphosed Neoproterozoic rocks. The Woxi W–Au–Sb deposit is an extremely large deposit with huge reserves of 0.25 Mt WO_3, 42 t Au, and 1.67 Mt Sb (Ten et al., 1999; Liu et al., 2000), and with>100 years of mining history (Kuang et al., 2004). The deposit is hosted in the Neoproterozoic Madiyi Formation of the Banxi Group. Mineralization mainly occurs as banded and network quartz veins with a small amount of altered breccias (Ten et al., 1999; Kuang et al., 2004). Previous studies revealed two stages of mineralization at Woxi with Caledonian (402 Ma ± 6 Ma) and Yanshanian ages (144.8 Ma ± 11.7 Ma) (Shi et al., 1993; Peng et al., 2003).

3. Deposit geology

3.1. Dahutang W deposit

The host rock of the Dahutang W deposit is mainly Neoproterozoic biotite granodiorite of the Jiuling batholith (820 Ma) (Li et al., 2003; Zhong et al., 2005; Zhang, 2013; Yang et al., 2014). There are three main stages of Yanshanian granites in the Dahutang W deposit (Fig. 2). The early stage is porphyritic biotite granite with an age of 147 to 150 Ma (Mao et al., 2015). The second stage is medium- to fine-grained granite

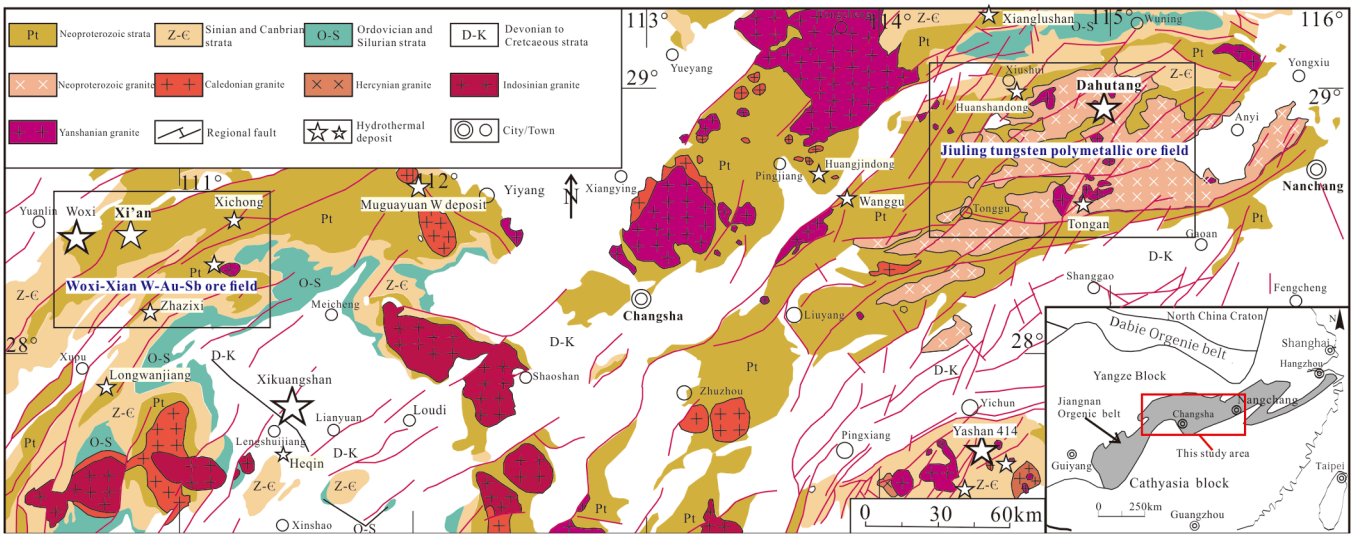

Fig. 1. Geological map of the Middle Jiangnan orogenic belt (after Ma et al. (2002) and Zhang (2018)).

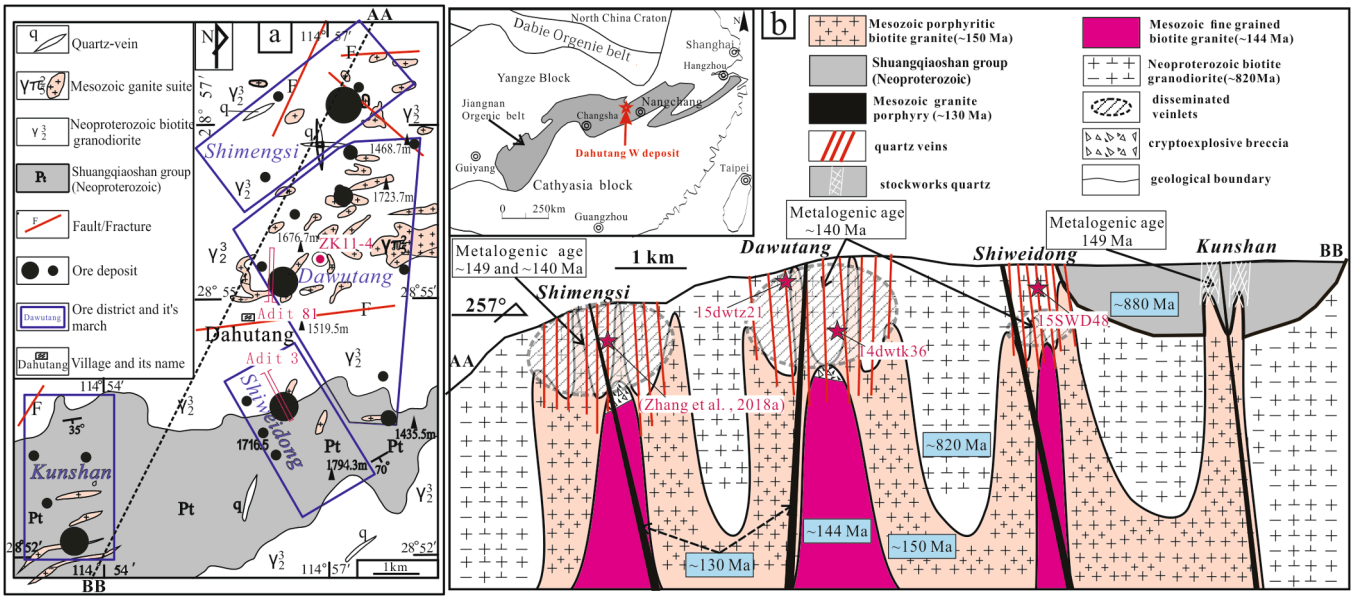

Fig. 2. (a) Geological sketch map of the Dahutang tungsten deposit, which includes the four mines Shimengsi, Dawutang, Shiweidong, and Kunshan and their mining boundaries. (b) Geological cross-section 'AA–BB' (through four segments) of the Dahutang tungsten deposit (modified from (Zhang et al., 2018b).

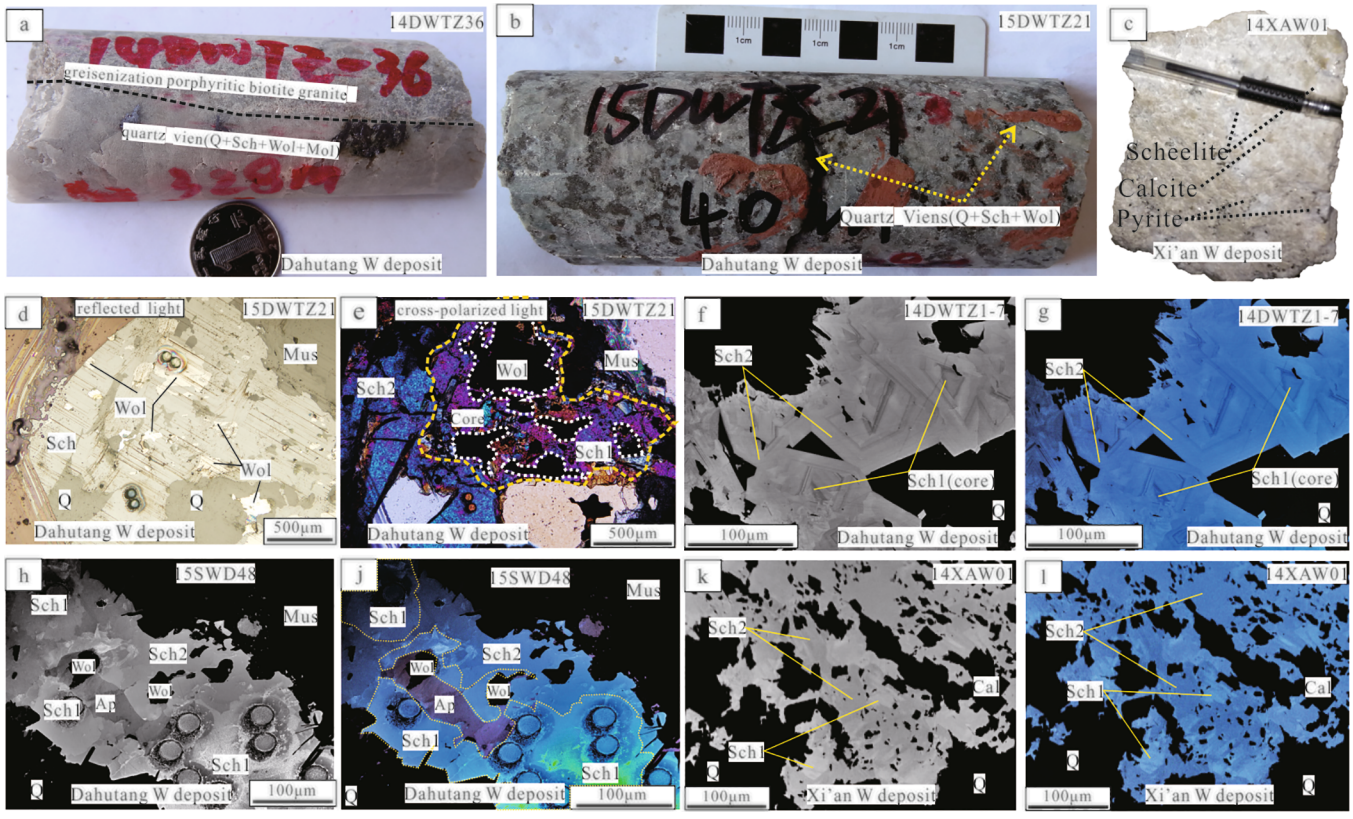

Fig. 3. Mineralogical characteristics of scheelite from the Dahutang and Xi'an tungsten deposits. (a) quartz veins and veinlet-disseminated type from the greisenization of porphyritic biotite granite; (b) stockworks from biotite alteration and greisenization of Neoproterozoic biotite granodiorite; (c) quartz veins (Xi'an deposit); (d) scheelite paragenetic with wolframite (Dahutang deposit); (e) scheelite core and border (Dahutang deposit); (f) oscillatory zoning of scheelite secondary electrons map (SEM) (Dahutang deposit); (g) oscillatory zoning of scheelite cathodoluminescence (CL) image (Dahutang deposit); (h) SEM of scheelite shows a two-stage mineralization (Dahutang deposit); (j) CL image of scheelite showing two-stage mineralization (Dahutang deposit); (k) SEM of scheelite showing two-stage mineralization (Xi'an deposit); (l) CL image of scheelite showing two-stage mineralization (Xi'an deposit). Q: quartz; Wol: wolframite; Sch1: scheelite stage 1; Sch2: scheelite stage 2; Mus: muscovite; Ap: apatite.

with an age of 144 to 146 Ma (Mao et al., 2015). The last stage is mainly granite porphyry and porphyry veins with zircon U–Pb ages of 140 to 130 Ma (Jiang et al., 2015).

Four alteration types have been recognized in the Neoproterozoic biotite granodiorite at Dahutang (Zhang et al., 2018b). I: Biotite alteration (biotitization), which is characterized by two types of biotite (re-equilibrated and hydrothermal biotite) accompanied by mineralization (mostly an assemblage of biotite ± wolframite ± apatite). II: Phyllic (fine-grained aggregate of muscovite (Li-phengite) ± quartz) alteration with hydrothermal alteration immediately after biotitization, with some sulfides deposited. III: Greisenization comprised of muscovite (zinnwaldite + Li-phengite) ± quartz + wolframite + scheelite ± sulfide. IV: Silicification (hydrothermal quartz and quartz veins) that overprinted the previous stages. Alkaline alteration (sodic, potassic, and greisenization) is locally overprinted by acidic alteration (silicification) in the porphyritic biotite granite (the inner contact zone), which plays an important role in the enrichment of W (Zhang et al., 2018b).

Tungsten mineralization is mainly distributed in the inner and outer zones of the contact between the Yanshanian porphyritic granite and Neoproterozoic biotite granodiorite (Fig. 3a and b). The reserves in the outer zone are larger than those in the inner zone (Xiang et al., 2013b; Zhang et al., 2017). The Neoproterozoic biotite granodiorite in the contact zone has been through extensive biotitization (potassic alteration). Tungsten mineralization is mostly concentrated in the biotite alteration zone (Zhang et al., 2018b, 2018c).

The Dahutang W deposit is composed of four segments: Shimensi, Dawutang, Shiweidong, and Kunshan (from the north to the south; Fig. 2a and 2b) (Zhang et al., 2018b). The Shimensi segment is the largest, with reserves of > 0.74 Mt WO_3 at grades of 0.195% (Xiang et al., 2013b). The Dawutang segment is located in the south of the Shimensi segment, with WO_3 reserves of > 0.25 Mt, the W orebodies of these two segments are mainly hosted in the Neoproterozoic biotite granodiorite (Zhang et al., 2017). The Shiweidong segment has WO_3 reserves of > 0.3 Mt (Feng et al., 2012). The Shiweidong W mineralization mainly occurs in the outer contact zone between the Yanshanian porphyritic biotite granite, Neoproterozoic biotite granodiorite and low-grade metamorphosed sedimentary strata (Feng et al., 2012). The Kunshan segment is a large Mo–Cu–W polymetallic deposit. The W mineralization mainly occurs in the outer contact zone between the Yanshanian porphyry biotite granite and the Shuangqiaoshan Group (Zhang et al., 2016). The W mineralization of the Dahutang deposit occurs as veinlet-disseminated, quartz vein type, and hydrothermal crypto-explosive breccia types (Xiang et al., 2013a, 2013b; Zhang et al., 2017).

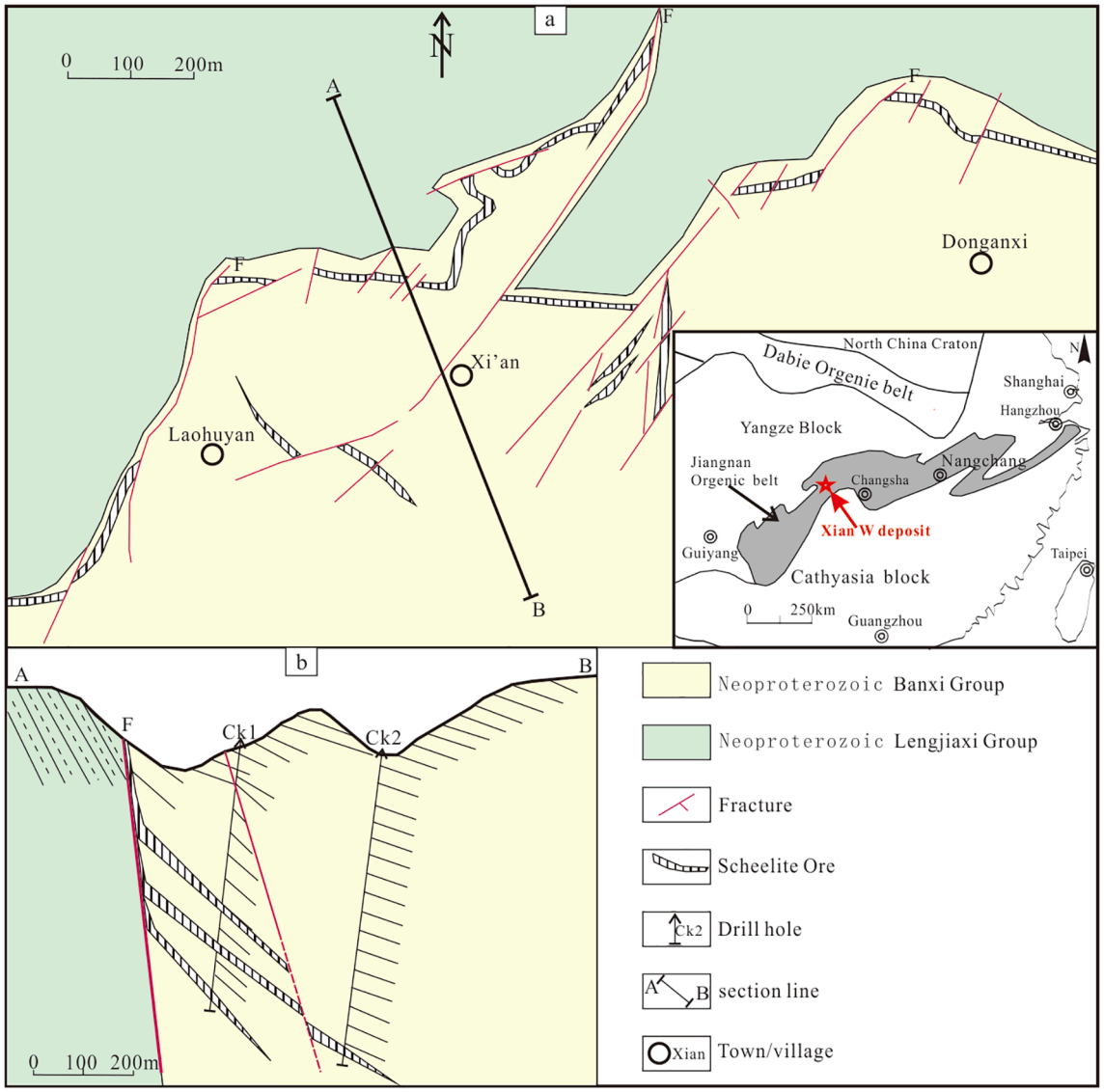

Fig. 4. Geological maps of (a) Xi'an tungsten deposit, and (b) the exploration line profile (He and Zeng, 1987).

3.2. Xi'an Au-W deposit

The Xi'an W deposit is located in the southern limb of the paleo Foshan overturned anticline, which is a secondary structure of the Xuefengshan Uplift belt in the Middle Jiangnan orogenic belt (Wan, 1986). The host rocks are the Neoproterozoic Banxi and Lengjiaxi groups (Fig. 4a and b). The Xi'an W deposit is mainly composed of purplish-red, grayish-green slate, and sandy siltstone. Several carbonate layers and limestone lenses between the lower part of the Banxi Group and the upper part of the Lengjiaxi Group host the orebodies of the Xi'an W deposit. Faults are well developed in this area, with an east–west trending fault being the main fault that runs through the entire Woxi–Xi'an Au–W–Sb ore field and controls the distribution of the deposits (Fig. 4a). The northeast, north-northeast, and north–south trending faults control the distribution of mineralization in the Xi'an W deposit. The intersection of the carbonate layer by fractures and a fracture zone is the most favorable location for ore precipitation. No igneous rock is exposed within 20–40 km of the deposit, and no evidence of concealed intrusions has been identified (Wan, 1986).

There are 11 quartz–calcite veins with W mineralization at the Xi'an W deposit (Wan, 1986), which are controlled by structure and lithofacies. Tungsten mineralization is mainly of the vein-network type, followed by the quartz vein type. The main minerals are scheelite, quartz, and calcite (Fig. 3e and f) as well as a small amount of chalcopyrite, pyrite, and native gold. Scheelite mainly occurs in the quartz and calcite veins. Some occurs as hydrothermal veins or breccia cement in fracture zones in carbonate areas, and also as a scheelite + quartz + calcite association in altered carbonates.

4. Analytical methods and results

4.1. Sampling and analytical methods

Scheelite samples from veinlet-disseminated and quartz vein types of mineralization in the altered Neoproterozoic granodiorite and Yanshanian porphyry biotite granite within the four segments of the Dahutang deposit were used in this study (Fig. 2b and Table 1). Scheelite samples from a quartz vein in the altered Neoproterozoic Banxi Group from the Xi'an W deposit were also analyzed (Fig. 3c and Table 1).

Quantitative chemical analyses of the scheelite samples were performed on polished thin sections using a JEOL JXA-8230 EMPA at the State Key Laboratory of Nuclear Resources and Environment, East China University of Technology, China. The operating conditions were set at a probe current of 20nA, an acceleration voltage of 15 kV for all elements, and a beam diameter of 1.0 μm for scheelite. Cathodoluminescence imaging was performed at 15 kV and 20nA using a CAMECA cathodoluminoscope. The CL was recorded as gray-scale images to document textures and zonation in scheelite.

Table 1
The scheelite sampling location and description from Dahutang and Xi'an Wdeposit.

	Sample	Location	Description
1	14dwtk36	From Dawutang segment quartz vein No. 53 , Adit 81, Elevation = 1340 m	Quartz vein side Greisenization altered Yanshanian porphyry biotite granite, disseminated ore sample. The quartz vein width 55 cm, dip angle 71°.
2	15dwtz21	From Dawutang segment the drill ZK11-4, E: 114°57′21.804″, N: 28°56′22.484″, sample elevation = 1601 m	Greisenization altered Neoproterozoic biotite granodiorite, disseminated ore.
3	15SWD48	From Shiweidong segment, the Adit 3, quartz vein No. 15-7, Elevation = 1170 m	Quartz vein side Greisenization altered Neoproterozoic biotite granodiorite, disseminated ore sample. Quartz vein width 3 cm, dip angle 30°.
4	14XAW02	From Xi'an W deposit, adit 3-3, quartz vein 5-1,	Quartz vein orebody, coarse-grained scheelite fossil quartz vein, scheelite 0.1–20 mm, quartz vein width 50 cm, tilt north-northwest, dip angle 65°.

The LA-ICP-MS analysis was performed by FocuMS Technology Co. Ltd., Nanjing, China. Laser sampling was performed using a Cetac Photon Machine with a 193 nm ArF excimer laser ablation system, coupled to an Agilent 7700x ICP–MS. A 40-um spot was used with an energy density of 5.6 J/cm^2 and a repetition rate of 5 Hz. The instrument settings were optimized by ablating the NIST SRM 610 standard to obtain high signal intensities but a low oxide content (ThO/Th < 0.3%) and doubly charged ion (Ba^{2+}/Ba^{+} < 0.4%) production. Each LA-ICP-MS analysis incorporated a ~15 s background acquisition (gas blank) and a 40 s data acquisition from each sample. Every nine-spot analyses were followed by a NIST SRM 610 analysis to correct the time-dependent drift of sensitivity and mass discrimination of the ICP–MS. Reference glasses (NIST612 and NIST610) were analyzed prior to and after the sample measurements. The NIST SRM 610 was used as the external standard and data reduction was performed using the ICPMS-DataCal software (Liu et al., 2008b). Raw data reduction was performed off-line with the ICPMSDataCal 10.1 software using the 100%-normalization strategy without applying an internal standard (Liu et al., 2008b). The standard deviation of the trace elements was better than ± 10%.

4.2. Results

4.2.1. Cathodoluminescence and mineralogy

The mineralogy of the scheelite samples from the Dahutang W deposit (Fig. 3) indicate at least two generations of scheelite in the veinlet-disseminated W mineralization. During the early stage, wolframite was surrounded by scheelite (D1), with a later generation of scheelite (D2) formed around the early scheelite stage (D1) (see Fig. 3c and d). Under the orthogonal polarizing microscope, D1 was observed to be dark purple, while D2 was dark blue. The two generations of scheelite from the Dahutang W deposit exhibit different CL characteristics; D1 had a dark blue CL (Fig. 3g, j), granular form and altered wolframite at the core of the scheelite grain (Fig. 3d, e). In contrast, D2 had a bright blue CL and encloses the D1 (Fig. 3e, g).

The scheelite from the Xi'an W deposit was observed to be gray-white under a microscope. The texture and mineral association suggest that scheelite in the Xi'an deposit includes at least two generations but with limited differences. The early generation (X1) had a bright blue CL and granular core (Fig. 3k, 3l), whereas the later generation (X2) had a dark blue CL and enclosed the early scheelite (Fig. 3e, 3g).

4.2.2. Trace element and REE composition

(1) Scheelite from the Dahutang W deposit

The Mo concentration of the early scheelite (D1) and late scheelite (D2) ranged from 27 ppm to 175 ppm and 36 ppm to 176 ppm, respectively (Table 2). Fig. 5a shows that the Nb + Ta concentration and total rare earth elements (ΣREE) contents of the D1 scheelite samples were relatively high compared to the Xi'an W deposit (Table 2). The Nb + Ta concentration of the D1 samples (28–133 ppm, mean of 74 ppm) from the Dahutang deposit is generally higher than that of the D2 samples (5.7–145 ppm, mean of 57 ppm), both of which are higher than the scheelite samples from the Xi'an tungsten deposit (1.0–1.3 ppm, mean of 1.2 ppm) (Fig. 5a). The plot of U + Th versus the ΣREE contents of the scheelite samples shows that the U + Th concentration of the D1 samples is lower than the Xi'an W deposit (Fig. 5b and Table 2). The U + Th concentration of the D1 samples (0.06–88 ppm, mean of 8.9 ppm) is lower than that of the D2 samples (0.3–44 ppm, mean of 11.9 ppm), and both are lower than the scheelite from the Xi'an W deposit (0.54–54

Table 2
EMPA and LA-ICP-MS analyses of major and trace elements in scheelite at the Dahutang and Xi'an tungsten deposit.

Sample	15swd48-02	15swd48-03	15swd48-05	15swd48-06	15swd48-13	14dwtk36-01	14dwtk36-02	14dwtk36-04	14dwtk36-05	15dwtz21-1-03	15dwtz21-1-04	15dwtz21-1-05
Segment/deposit	Shiweidong	Shiweidong	Shiweidong	Shiweidong	Shiweidong	Dawutang	Dawutang	Dawutang	Dawutang	Dawutang	Dawutang	Dawutang
Generation	D1	D1	D1	D1	D1	D1	D1	D1	D1	D1	D1	D1
EMPA (wt%)												
WO_3	78.39	79.69	78.80	78.49	78.54	79.87	78.75	79.33	80.97	80.14	80.55	80.25
SiO2	0.22	0.22	0.27	0.23	–	–	0.25	–	–	–	0.21	–
CaO	19.40	19.70	19.46	19.30	19.28	19.45	19.62	19.50	19.51	19.51	19.58	19.55
Na_2O	–	–	–	0.02	0.02	0.05	0.04	0.06	0.02	–	–	0.01
MoO_3	0.07	0.04	–	0.10	0.05	–	0.01	0.03	–	–	0.13	–
F	0.01	–	–	0.02	–	–	0.01	–	0.04	0.02	0.01	0.05
SrO	–	–	–	–	–	–	–	–	–	–	–	–
FeO	–	0.02	0.03	0.09	0.04	–	0.09	0.01	0.01	0.03	0.06	0.05
MnO	0.03	0.02	–	0.03	–	0.01	–	–	–	–	–	0.02
P_2O_5	0.08	0.07	0.07	0.05	0.09	0.07	0.10	0.07	0.04	0.06	0.03	0.07
Total	98.20	99.76	98.63.	98.32	98.01	99.46	98.87	99.00	100.58	99.76	100.57	99.99
LA-ICP-MS (ppm)												
Cr	0.38	2.9	1.2	1.2	3.4	2895	29.9	87	11.8	14.2	3.4	13.5
Ni	0.19	0.21	0.14	0.02	0.09	1.39	0.01	0.03	0.05	0.03	–	0.22
Cu	0.11	0.19	–	0.02	0.04	3.64	3.32	0.03	–	0.44	0.11	0.17
Zn	0.24	0.57	3.28	1.64	–	1.72	0.65	3.56	–	0.49	0.37	1
Mo	155	132	157	154	175	48	50	34	37	39	38	27.2
Sn	3.4	3.3	6.5	2.78	2.65	0.78	0.93	0.67	0.64	2.89	3	3.4
Rb	0.04	0.91	0.14	0.69	0.15	1.1	5.4	0.05	0.03	0.1	0.03	0.17
Sr	44	63	77	68	65	54	51	55	55	78	78	95
Zr	0.02	0.02	0.06	0.01	0.01	0.1	0.04	0.05	0.04	0.03	0.01	0.03
Hf	0.01	0.04	0.03	–	–	0.02	0.02	0.02	0.02	0.01	–	0.01
Nb	115	95	27.3	113	27.0	78	53	60	45	67	56	129
Ta	4.8	4.0	1.06	3.9	0.9	1.3	1.17	1.01	0.94	1.36	0.88	3.4
Ba	0.07	0.21	0.7	0.04	0.1	0.51	2.95	0.27	0.12	0.13	0.09	0.41
Th	0.28	0.41	86	9.9	1.41	0.03	0.08	0.02	0.02	0.9	0.18	0.39
U	0.19	0.15	1.43	1.31	0.44	2.11	0.21	0.08	0.04	0.27	0.11	0.29
Pb	29.5	38	29.2	34	26.0	24.8	17.0	18.4	20.3	15.6	14.8	15.2
Y	789	1140	1002	355	611	503	596	496	564	454	374	449
Au	0.53	0.84	0.68	0.69	0.69	0.63	0.67	0.74	0.75	0.72	0.76	0.69
Sb	–	0.07	–	0.09	–	1	0.1	0.03	0.04	–	–	0.07
Nb + Ta	120	99	28	117	28	80	54	61	46	69	57	133
U + Th	0.47	0.56	87.69	11.21	1.85	2.14	0.29	0.1	0.06	1.17	0.29	0.68

Sample	15SWD48-04	15SWD48-07	15SWD48-08	15SWD48-11	15SWD48-12	15dwtz21-1-01	15dwtz21-1-02	15dwtz21-2-03	15dwtz21-2-04
Segment/deposit	Shiweidong	Shiweidong	Shiweidong	Shiweidong	Shiweidong	Dawutang	Dawutang	Dawutang	Dawutang
Generation	D2	D2	D2	D2	D2	D2	D2	D2	D2
EMPA (wt%)									
WO_3	79.06	79.32	79.07	79.01	78.36	79.21	79.08	80.02	81.10
SiO2	–	–	–	0.11	–	0.22	–	0.25	0.21
CaO	19.36	19.43	19.51	19.58	19.68	19.57	19.59	19.54	19.78
Na_2O	–	0.01	–	–	–	0.01	0.02	–	–
MoO_3	0.14	–	0.10	0.03	0.02	0.14	0.12	0.10	–
F	0.01	–	0.03	–	–	0.07	0.01	–	–
SrO	–	–	–	–	–	–	–	–	–
FeO	–	0.05	–	0.41	0.03	0.07	0.05	0.02	–
MnO	0.04	0.01	–	–	0.01	–	0.11	0.01	0.02
P_2O_5	–	0.04	0.03	0.06	0.07	0.09	0.02	–	–
Total	98.60	98.87	98.72	99.19	98.18	99.35	98.99	99.94	101.12
LA-ICP-MS (ppm)									
Cr	0.61	1	–	1.14	1.69	0.94	0.89	19.4	4.1
Ni	0.08	0.17	0.1	–	0.05	0.05	0.05	0.11	0.23
Cu	–	–	0.22	0.23	0.03	–	–	0.05	–
Zn	0.39	0.59	0.45	0.57	–	0.12	–	0.95	–
Mo	121	155	157	176	140	167	148	43	36
Sn	2.9	3.2	3.1	2.2	2.3	2.7	3.6	2.1	2.8
Rb	0.21	0.09	0.02	0.05	0.06	0.05	0.06	0.1	0.01
Sr	59	69	79	170	96	62	73	90	95
Zr	0.01	0.02	0.01	0.01	0.01	0.01	0.01	0.03	–
Hf	0.02	–	0.01	–	–	0.01	–	0.01	–
Nb	139	12.6	26.0	5.5	83	9.8	130	46	44
Ta	5.4	0.39	1	0.18	3.7	0.24	3.7	1.05	1.11
Ba	–	0.02	0.05	0.16	0.06	–	0.09	0.09	–
Th	0.2	5.9	22.9	35.2	0.51	7.42	13.4	0.36	0.16
U	0.1	1.75	4.82	9.13	0.18	2.00	1.69	0.2	0.13
Pb	26.2	29.9	31.0	29.5	22.1	28.3	39	16.3	17.0
Y	980	578	376	271	678	369	181	315	249
Au	0.66	0.65	0.91	0.72	0.89	0.74	0.7	0.74	0.74
Sb	0.04	–	0.1	–	–	0.06	0.17	–	0.14
Nb+Ta	145	13.0	27.0	5.7	87	10.1	134	47	45
U+Th	0.3	7.7	27.7	44.3	0.69	9.4	15.1	0.56	0.29

Sample	14xaw-1-01	14xaw-1-02	14xaw-2-03	14xaw-2-01	14xaw-1-03	14xaw-2-04	14xaw-2-02	14xaw-2-05
Deposit	Xi'an	Xi'an	Xi'an	Xi'an	Xi'an	Xi'an	Xi'an	Xi'an
Generation	X1	X1	X1	X2	X2	X2	X2	X2
EMPA (wt%)								
WO_3	79.82	80.96	81.46	80.26	78.87	81.65	80.05	79.61
SiO2	–	0.20	0.21	–	0.21	–	0.20	–
CaO	20.05	20.37	19.82	20.01	20.28	18.06	20.25	20.12
Na_2O	0.01	0.03	0.01	–	–	–	0.01	–
MoO_3	–	0.20	0.01	–	–	0.06	0.03	–
F	–	–	–	–	–	–	–	–
SrO	–	–	–	–	–	–	–	–
FeO	0.02	–	0.03	–	–	0.08	0.02	0.07
MnO	–	–	0.01	–	0.01	0.04	–	–
P_2O_5	–	0.04	0.04	0.01	0.05	0.04	0.05	0.01
Total	99.90	101.79	101.60	100.29	99.42	99.93	100.61	99.81
LA-ICP-MS (ppm)								
Cr	18.0	14	0.27	0.97	32	0.29	1.79	4.4
Ni	0.09	0.16	0.11	–	0.17	0.06	0.1	–
Cu	0.02	0.06	–	0.01	0.12	–	0.13	0.18
Zn	1.46	0.13	0.21	0.18	0.08	–	0.12	0.09
Mo	1.48	1.49	3.42	3.84	1.77	1.58	2.03	3.21
Sn	0.31	–	–	0.49	–	0.87	0.01	0.84
Rb	0.35	0.38	0.03	–	0.04	0.09	0.02	–
Sr	861	715	640	718	873	582	614	707
Zr	0.07	0.02	0.04	0.06	0.08	0.03	0.01	0.1
Hf	0.03	0.07	0.01	–	–	0.01	–	–
Nb	1.29	1.19	1.00	1.24	1.15	1.20	1.09	1.11
Ta	0.02	0.02	0.01	0.01	0.02	0.01	0.01	0.04
Ba	0.03	0.19	0.05	0.09	0.83	0.18	0.07	0.17
Th	0.04	0.05	0.13	0.1	0.06	0.16	0.23	0.11
U	3.8	0.49	11.7	36	21.8	0.17	9.5	54
Pb	86	28	42	61	71	20.3	36	53
Y	975	1007	275	10.7	501	567	174	22.7
Au	0.61	0.66	0.71	0.73	0.65	0.74	0.66	0.65
Sb	0.09	0.47	0.28	1.64	5.24	2.26	8.22	1.77
Nb+Ta	1.31	1.21	1.01	1.25	1.17	1.21	1.10	1.15
U+Th	3.82	0.54	11.85	36	21.8	0.33	9.75	54

"-" means under the detection limit.

ppm, mean of 17.3 ppm) (Fig. 5a).

The D1 scheelite samples have a relatively high abundance of ΣREE (779–2561 ppm), a light REE/heavy REE (LREE/HREE) ratio of 4.33–10.7, and a La_N/Yb_N ratio of 41.5–196 (Table 3 and Fig. 6b). The δEu values of the D1 samples ranged from 0.17 to 0.85 with negative anomalies (Table 3 and Fig. 6b). The D2 samples exhibited lower REE contents (147–1068 ppm), a LREE/HREE ratio of 3.55–8.63, and a La_N/Yb_N ratio of 80–195. The δEu values of the D2 samples ranged from 1.16 to 9.51, with positive anomalies (Table 3 and Fig. 6c).

The REE characteristics for the two stages of scheelite are quite different (Fig. 6b). During the early scheelite stage, the scheelite (core) exhibits negative Eu anomalies, and the LREEs and HREEs were not differentiated. The REE distribution curve of the D2 scheelite samples exhibited positive Eu anomalies (Fig. 6c).

(2) Scheelite from the Xi'an W deposit

The scheelite samples from the Xi'an tungsten deposit have relatively low Mo concentrations (1.48–3.84 ppm) (Table 2), lower than that of the D1 and D2 samples. The scheelite from Xi'an W contains ΣREE contents of 11.8–983 ppm, lower than the scheelite samples from the Dahutang W deposit. The LREE/HREE ratio varies from 0.08 to 3.24, and the La_N/Yb_N ratio from 0.23 to 91. The scheelite samples from the Xi'an W deposit have δEu values of 0.76–1.14 (Table 3). The ΣREE contents decreased from the core of the scheelite (X1) towards the rim (X2) (Fig. 6a).

The REE characteristics of the X1 samples is similar to that of the samples from the Woxi Au–Sb–W deposit, with no obvious Eu anomalies or relative loss of LREEs and HREEs, but an enrichment of medium REEs (MREEs). However, the X2 samples were characterized by lower MREE contents but enriched LREEs and HREEs.

5. Discussion

The four alteration types of the Dahutang W deposit have recorded physicochemical information regarding the transformation of ore-forming fluids into hydrothermal minerals (e.g., hydrothermal biotite, muscovite, scheelite, and quartz). A high oxygen fugacity (fO_2) of the hydrothermal fluid would inhibited the formation of wolframite or the decomposition of early wolframite, but would be beneficial to the formation of scheelite (Liu and Ma, 1987a). The chemical composition of hydrothermal alteration and biotite suggest that a high oxygen fugacity during biotitization ($Log(fO_2)$ = -13.6 to −14.1) was unfavorable for wolframite deposition (Zhang et al., 2018b). As the oxygen fugacity decreased during the early greisenization ($Log(fO_2)$ = -17.6 to −17.8) process, wolframite could precipitate from the hydrothermal fluids (Zhang et al., 2018b). The formation of abundant scheelite requires a high $f(O_2)$ and a sufficient Ca concentration in the hydrothermal fluid (Liu and Ma, 1987a). Hence, the $f(O_2)$ and composition of the ore-forming fluids that formed the later greisenization (mostly scheelite, Li-phengite and some quartz) must change. The Eu anomalies of scheelite record the physicochemical characteristics of the fluid, especially the $f(O_2)$ (Brugger et al., 2008).

The Woxi-Xi'an Au–Sb–W ore field is an important stratabound Au–Sb–W metallogenic belt. The Woxi Au–Sb–W and Xi'an Au–W deposit are mainly hosted by Neoproterozoic strata, and formed during the Caledonian and Yanshanian. The ore-forming materials of the Xi'an Au–W and Woxi Au–Sb–W deposits were mainly formed by the leaching the Neoproterozoic wall rock, primarily with an ore-forming fluid of a metamorphic-origin (Wan, 1985; Ten et al., 1999; Liu et al., 2000). Previous work has confirmed that the ore-forming fluid of the Woxi Au–Sb–W and Xi'an Au–W deposit originated from metamorphic fluids mixed with deep cycling seawater (Wan, 1985, 1986; Zhang, 1985; Ma and Liu, 1992; Gu et al., 2005; Peng et al., 2006). Hence, W, Au, and Sb were leached from the Neoproterozoic strata by the infiltration of meteoric fluids at depth, which mixed with the metamorphic fluid, leading to the formation of a regional geochemical negative gold

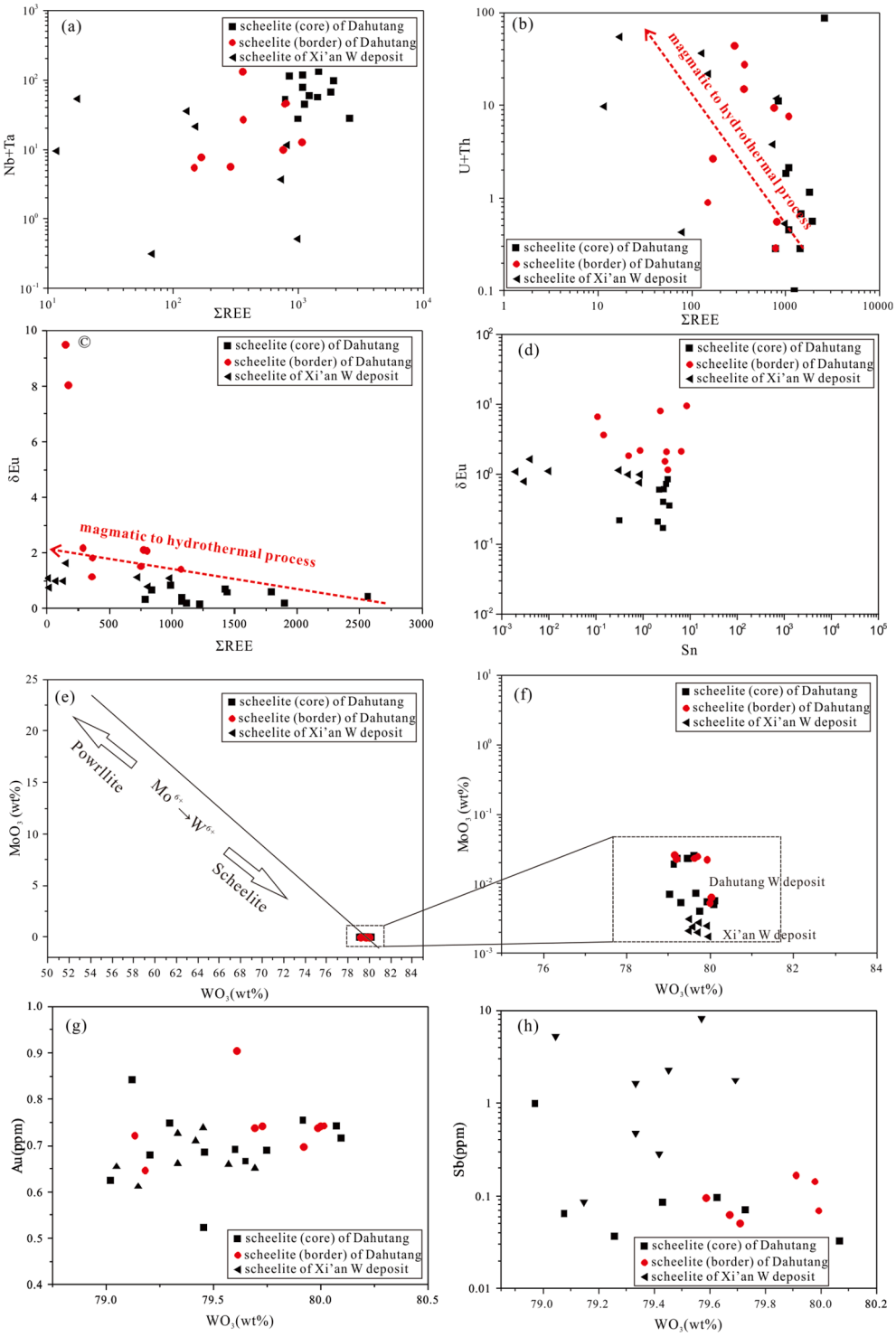

Fig. 5. Trace element characteristics of scheelite from the Dahutang and Xi'an tungsten deposits (the scheelite data for Huangshaping are from Ding et al. (2018)).

anomaly zone (Ma and Liu, 1991, 1992; Niu and Ma, 1992; Liu et al., 1993). The fluid further evolved into an ore-forming fluid before migrating to the favorable ore-forming structure, and then precipitated to form the deposit (Ma and Liu, 1991, 1992; Niu and Ma, 1992; Liu et al., 1993; Zhang et al., 2018d). Geochronology shows that the age of the Woxi-Xi'an Au-Sb-W ore field is Caledonian (402 ± 6 Ma) and Yanshanian (144.8 ± 11.7 Ma) (Shi et al., 1993; Peng et al., 2003). The two mineralization ages correspond to the Devonian and Cretaceous magmatism respectively in the Middle Jiangnan orogenic belt (Zhang, 2018).

Thus, both the Dahutang and Xi'an W deposits were mainly formed by a tectonomagmatic event (magmatic-hydrothermal or magmatic-heat) in the Middle Jiangnan orogenic belt. The scheelite of the Xi'an W deposits mainly formed as the result of magmatic heat driving metamorphic fluids that had mixed with deep cycling seawater. After investigating the chemical composition of the scheelite samples from the Dahutang and Xi'an W deposits, we propose that the $f(O_2)$ changed during the evolution of the Dahutang W deposit. In addition, the trace element characteristics of the scheelite from Dahutang and Xi'an W deposits may provide a new perspective to understand the ore-forming

Table 3
LA-ICP-MS analysis of REE in scheelite from the Dahutang and Xi'an tungsten deposits (ppm).

Sample	15SWD48-02	15SWD48-03	15SWD48-05	15SWD48-06	15SWD48-13	15dwtz21-1-03	15dwtz21-1-04	15dwtz21-1-05	14dwtk36-01	14dwtk36-02	14dwtk36-04	14dwtk36-05	15SWD48-04	15SWD48-07	15SWD48-08
Generation	D1	D1	D1	D1	D1	D1	D1	D1	D1	D1	D1	D1	D2	D2	D2
La	90	133	481	153	161	256	220	193	69	39	54	58	255	86	60
Ce	282	438	952	310	338	714	559	516	284	151	238	241	405	108	88
Pr	45	71	109	37	42	84	68	66	50	26	48	44	39	10	8.4
Nd	224	422	438	148	167	357	281	278	249	144	299	251	133	31	31
Sm	71	145	102	35	41	79	59	71	85	60	129	105	28	8.5	8.8
Eu	8.4	14.0	18.3	8.6	13.9	17.4	14.9	16.3	14.0	10.2	9.5	9.4	15.8	7.7	8.2
Gd	90	198	109	33	46	72	50	73	99	94	168	133	30.6	14.5	11.3
Tb	15.0	32	17.9	5.2	8.0	11.7	8.7	12.6	16.9	17.4	26.3	22.5	5.8	3.2	2.2
Dy	99	199	117	33	52	70	55	80	102	113	142	131	39	24.8	17.1
Ho	21.6	42	26.2	7.5	12.1	14.3	11.0	16.1	18.7	23.1	22.8	23.2	9.5	6.2	4.3
Er	58	106	77	22.5	39	43	35	46	47	57	49	54	32	21	14.1
Tm	8.2	12.9	11.8	3.9	6.5	7.8	6.4	7.8	6.0	6.6	5.1	6.2	6	3.4	2.6
Yb	53	75	89	34	53	59	47	52	32	34	26	31	59	30	24.3
Lu	6.3	9.2	13.4	5.6	8.0	7.7	5.9	6.6	4.0	4.0	2.7	3.7	10.2	5.1	4.1
ΣREE	1071	1897	2561	837	988	1793	1421	1435	1077	779	1218	1113	1068	360	284
LREE	641	1064	1980	648	708	1411	1128	1054	652	359	639	594	832	235	187
MREE	284	587	364	115	161	251	188	252	317	295	474	400	119	59	48
HREE	147	246	218	73	119	131	105	129	108	124	105	119	117	66	49
LREE/HREE	4.37	4.33	9.09	8.83	5.97	10.74	10.73	8.15	6.03	2.89	6.08	5.01	7.1	3.6	3.8
La_N/Yb_N	62	64	196	163	111	159	169	134	78	41	76	67	156	102	90
δEu	0.28	0.22	0.46	0.68	0.85	0.61	0.73	0.6	0.4	0.36	0.17	0.21	1.4	1.8	2.2

Sample	15SWD48-11	15SWD48-12	15dwtz21-1-01	15dwtz21-1-02	15dwtz21-2-03	15dwtz21-2-04	14xaw-1-01	14xaw-1-02	14xaw-2-03	14xaw-2-01	14xaw-1-03	14xaw-2-04	14xaw-2-02	14xaw-2-05
	D2	D2	D2	D2	D2	D2	X1	X1	X1	X2	X2	X2	X2	X2
La	193	83	147	137	23	31	0.82	0.39	0.16	2.23	2.34	3.3	4.2	7.1
Ce	298	146	324	311	44	55	3.9	3.4	2.21	4.0	3.4	8.3	2.6	3.5
Pr	28	13.6	33	34	4.9	5.5	1.94	2.05	2.84	1.03	0.67	2.03	0.35	0.44
Nd	87	46	105	106	17	18	17.0	20.8	51	6.1	2.47	8	1.10	1.10
Sm	17.4	10.4	21	21.3	4.2	4.3	27.1	45	89	4.6	0.81	1.56	0.16	0.08
Eu	10.3	4.2	15.8	16.9	16.2	13.5	22.0	35	42	2.60	0.96	0.74	0.10	0.02
Gd	18.5	8.9	19	20.9	5	4.6	97	162	229	10.6	3.0	3	0.35	0.09
Tb	3.3	1.6	4.2	4.4	1.10	1.00	30	46	39	3.0	1.47	0.55	0.05	0.01
Dy	24.6	11.6	32.4	34.5	8.5	8.7	239	343	214	27.3	19.7	7	0.35	0.20
Ho	5.6	2.7	7.4	7.1	1.9	2	52	68	36	7.1	6.7	1.95	0.08	0.05
Er	19.6	9	26.6	24.6	6.8	7.1	137	161	71	25	32	9	0.28	0.30
Tm	3.8	1.8	5.5	5.1	1.3	1.6	17.0	17.6	6.5	4.2	7.5	2.18	0.10	0.20
Yb	36	17	48	43	10.6	12.5	76	73	24.8	27.5	61	18	1.67	3
Lu	6	2.9	6.5	5.9	1.6	1.8	7.5	6.5	2.19	3.4	8.3	2.8	0.42	0.83
ΣREE	750	358	796	772	146	166	728	983	809	128	151	68	11.8	17.3
LREE	605	288	609	588	89	109	23.7	26.7	56	13.3	8.8	21.3	8.3	12.1
MREE	74	37	92	98	35	32	415	631	613	48	25.9	12.0	1.01	0.39
HREE	71	33	94	86	22	25	290	325	140	67	116	35	3	5
LREE/HREE	8.5	8.6	6.5	6.8	4	4.4	0.08	0.08	0.4	0.2	0.08	0.62	3.2	2.53
LaN/YbN	195	176	110	115	80	91	0.39	0.19	0.23	2.94	1.39	6.55	91	75
δEu	1.5	1.2	2.1	2.1	9.5	8	1.14	1.09	0.79	0.99	1.64	0.99	1.11	0.76

"-" means under the detection limit.

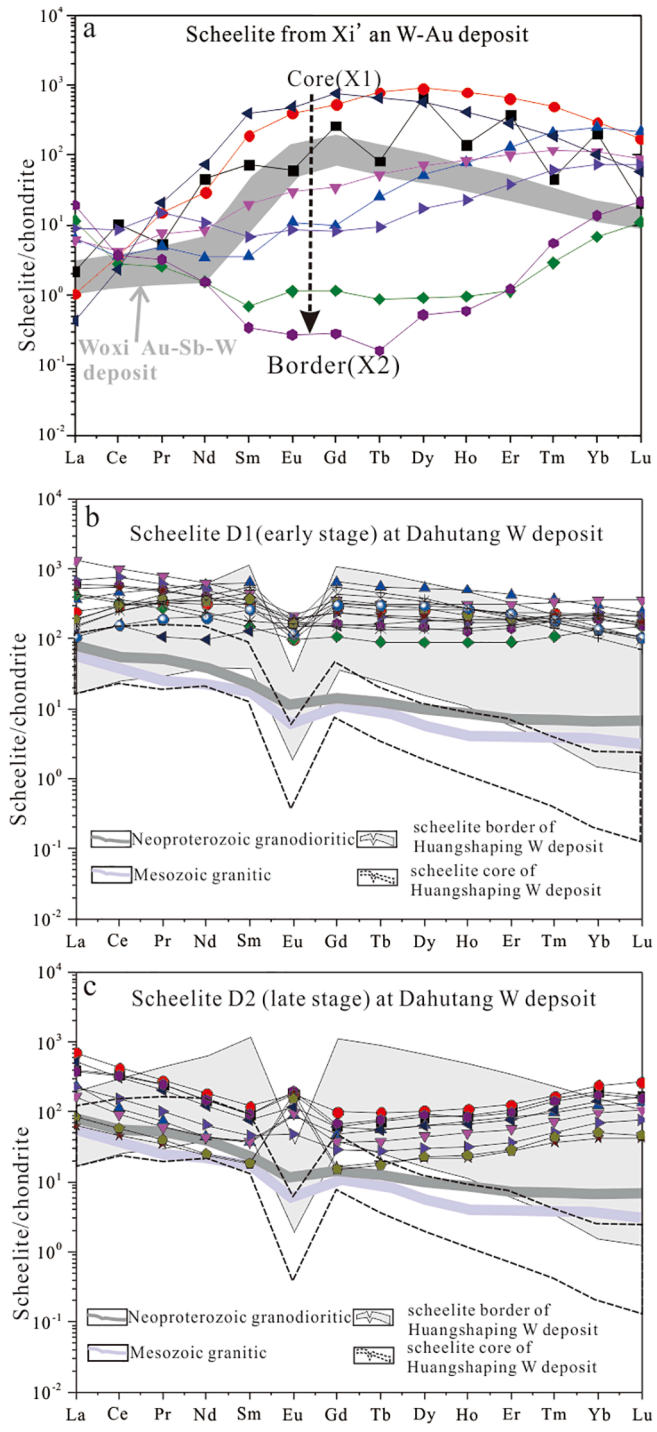

Fig. 6. Rare earth element (REE) distribution diagrams of (a) scheelite from the Xi'an deposit (Woxi data from Peng et al. (2005)), (b) of early scheelite (core) from the Dahutang deposit, and (c) scheelite (border) from the Dahutang deposit (the REE data of Neoproterozoic granodiorite and Mesozoic granite are from Zhang et al. (2018c)).

fluids of the Dahutang W deposit.

5.1. The source of ore-forming fluids of Dahutang W deposit

Ore-forming fluids in the Earth's crust have three major sources (Dolejš and Wagner, 2008): (1) meteoric fluid, groundwater/seawater, and basinal fluids (Cathles, 1990; Gleeson and Yardley, 2003; Gleeson et al., 2003) that are enriched with Na, K, Ca, Mg, Cl^-, SO_4^-, and HCO_3^- (Demicco et al., 2005). (2) Metamorphic fluids produced by metamorphic dehydration and decarbonation reactions (Connolly and Thompson, 1989; Hanson, 1992; Kerrick and Connolly, 1998; Wing and Ferry, 2002), which are characterized by low granitophile element concentrations and high Sr and Ba concentrations (Van Daele et al., 2018). (3) Magmatic hydrothermal fluids formed from volatiles released from crystallizing magmas (Holland, 1972; Burnham, 1979; Carroll and Webster, 1994). Magmatic-hydrothermal fluids associated with W–Sn mineralization would be enriched in Na, Li, As, Nb, Mo, Sn, Sb, Ta, and W (Eugster, 1985; Liu and Cao, 1987; Bottrell and Yardley, 1988; Dolejš and Wagner, 2008).

The trace element composition of scheelite can be used to identify the source and evolution of ore-forming fluids (Sun and Chen, 2017; Zhang et al., 2018a; Zhao et al., 2018). The relatively high Na, Nb, Ta, and Mo concentrations but low Sr concentrations of the D1 scheelite (Fig. 7a, Table 2) suggest a magmatic hydrothermal fluid origin (Eugster, 1985; Liu and Cao, 1987; Bottrell and Yardley, 1988; Dolejš and Wagner, 2008). The stable isotope compositions of the ore-forming fluids ($\delta^{18}O_{fluid}$ = 5.4‰ to 8.8‰ and δD = −102‰ to −75‰) (Song et al., 2018) suggest that the magma-derived fluids were exsolved from the Late Jurassic granites at Dahutang. In contrast, the scheelite samples from the Xi'an deposit are characterized by relatively low Na, Nb, Ta, and Mo concentrations but high Sr, indicating a non-magmatic source. Previous studies of the ore-forming fluids of the Woxi and Xi'an deposits reported that they were mainly metamorphic fluids mixed with deep cyclic seawater (Wan, 1985; Ma and Liu, 1992; Niu and Ma, 1992; Liu et al., 1993; Peng et al., 2003, 2006). The variation in Eu concentration versus Sr of scheelite can also be used to trace the source of ore-forming fluids (Fig. 8a). The scheelite samples from the Xi'an deposit plot on a mixing line of metamorphic fluids and meteoritic water, consistent with the mixed source suggested in the previous studies.

Antimony is sensitive to the temperature of the ore-forming fluids, the higher the temperature, the greater the solubility of Sb in the fluid (Biver and Shotyk, 2013; Watson and Baxter, 2007). Therefore, the Sb concentration of scheelite may reflect the composition or temperature of the ore-forming fluid. The Sb concentration of the scheelite samples from the Dahutang deposit is very low (<1 ppm, mostly < 0.1 ppm), supporting a magmatic origin. In contrast, the scheelite samples, especially the X2 samples from the Xi'an deposit, have a relatively high Sb concentration (Fig. 5h), which is consistent with its precipitation from low-temperature fluids (c.f. Biver and Shotyk, 2013; Wilson et al., 2007).

In summary, the scheelite (D1) chemical composition reveal that the Dahutang deposit was formed by magmatic hydrothermal fluids, whereas the Xi'an deposit was formed by a low-temperature mixed fluid (metamorphic fluid with recycled meteoric water).

5.2. The evolution of ore-forming fluids of Dahutang and possible controls

Multi-generations of scheelite are ubiquitous in veinlet-disseminated W deposits in the Jiangnan Orogenic Belt. For example, the Muguayuan W deposit in the Middle Jiangnan orogenic belt, about 120 km away from the Xi'an W deposit (Fig. 1), is characterized by veinlet-disseminated W mineralization that developed in the Sanxianba granitic porphyry stock. The Muguayuan W deposit is formed by two stages (Li et al., 2018). From Stages I to II, scheelite Mo and Mn contents show a nearly linear change, which might have been caused by the successive precipitation of hydrothermal minerals (Li et al., 2018). The precipitation of molybdenite would significantly decrease Mo concentration in ore-forming fluids, leading to the precipitation of low-Mo scheelite in the later stages of mineralization of Muguayuan deposit (Li et al., 2018). Two generations of scheelite in the Dahutang W deposit have similar Mo concentrations (27.6 to 176 ppm), which are lower than the stage I scheelite (189 to 3420 ppm) of the Muguayuan W deposit, but higher than that of the stage II scheelite (0 to 1.85 ppm) (Li et al., 2018). Two generations of scheelite have similar Mo contents, indicating that

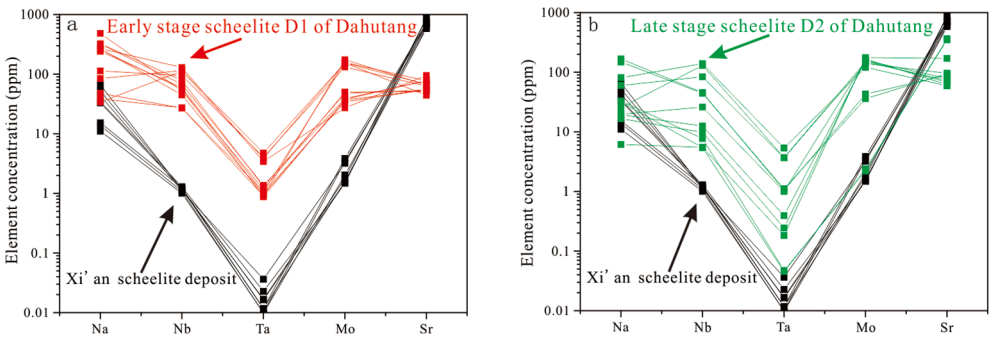

Fig. 7. Concentrations of Na, Nb, Ta, Mo, and Sr in scheelite samples from the Dahutang and Xi'an tungsten deposits. (a) Characteristics of a high Na, Nb, Ta, and Mo concentrations, and a low Sr concentration in the scheelite (core) from the Dahutang deposit; scheelite samples from the Xi'an deposit are characterized by a low Na, Nb, Ta, and Mo concentration, and a high Sr concentration. (b) The concentration of Na, Nb, Ta, Mo, and Sr in scheelite (border) from the Dahutang deposit are between that of the scheelite (core) from the Dahutang deposit and the scheelite from the Xi'an deposit.

no molybdenite precipitated during the formation of these two generations at the Dahutang W deposit. Low-Mo contents of scheelite result from a low Mo concentration ore-forming fluid.

The early generation scheelite (D1) has higher Na, Nb, and Ta but lower Sr than the late stage (D2) samples (Fig. 7). Thus, it is likely that the fluids that formed the D1 scheelite were magmatic hydrothermal fluids with high Na, Nb, and Ta concentrations but a low Sr concentration, whereas the fluids that precipitated the D2 scheelite had relatively low Na, Nb, Ta, and higher Sr concentrations. Molybdenum tends to be enriched in magmatic hydrothermal fluids (Audétat and Pettke, 2003). In addition, Nb and Ta are often enriched in scheelite or Nb–Ta-rich oxides (e.g., rutile). The lack of oxides in the scheelite-bearing veins suggests that the decreased Nb + Ta concentration was not caused by the fractionation of such oxides. The D1 scheelite samples had high Nb + Ta concentration, hence, crystallization of such an Nb–Ta-rich scheelite would result in a significant depletion of Nb and Ta in the evolved fluids.

The D2 scheelite samples of the Dahutang W deposit have higher Sr contents than the D1 scheelite, suggesting that the later stage (D2) fluids contained more Sr than the early stage (D1) fluids. The early stage (D1) fluids of the Dahutang deposit are characterized by a high Nb, Rb/Sr ratio but low Sr concentration (Table 2, Fig. 7), which is similar to the fluid of the typically magmatic hydrothermal W–Sn mineralization system (Eugster, 1985; Liu and Cao, 1987; Bottrell and Yardley, 1988; Dolejš and Wagner, 2008). The early stage (D1) fluids of the Dahutang deposit may have been derived from a highly fractionated granite resulting in a low Sr concentration. The association between the D1 scheelite and apatite (Fig. 3) is consistent with the Sr-depleted nature of the ore-forming fluids during the early stage. Strontium is compatible in both apatite and scheelite; hence, the crystallization of apatite and scheelite would lower the Sr concentration of the hydrothermal fluids (Brugger et al., 2000b; Prowatke and Klemme, 2006).

The higher Sr concentration of the D2 scheelite samples from the Dahutang deposit are similar to the scheelite samples from the Xi'an tungsten deposit (Fig. 8a). The Sr concentration of the fresh (unaltered) Neoproterozoic granodiorite varies from 72 to 200 ppm (mean = 110 ppm), whereas Sr concentration of the biotitization + greisenization altered granodiorite ranges from 19 to 85 ppm (mean = 44 ppm) (Zhang et al., 2018c). Consequently, the later stage (D2) fluids could not be derived solely by the evolution of the ore-forming fluids. Therefore, a Sr-rich source would have been required to form the high-Sr fluids during D2, such as an oxidized fluid formed after the fluid-rock interaction with a higher Sr wall rock such as the Neoproterozoic granodiorite.

The W mineralization of the Dahutang deposit is associated with extensive alkaline alteration. The Yanshanian granites have a relatively low Sr concentration; hence, the alteration of these granites would not account for the contribution of Sr to the evolved fluids (Zhang et al., 2018c). In contrast, the altered Jiuling granodiorites have lower Ca and Sr concentrations than the fresh rock (Zhang et al., 2018c), likely due to the decomposition of plagioclase. This suggests that Ca and Sr were leached out during the alteration of Neoproterozoic granodiorite (Zhang et al., 2018c).

The scheelite in the Dahutang deposit is characterized by an increasing Sr concentration with increasing elevation (Fig. 2b and 8b). The scheelite samples from the Shiweidong segment have higher Sr concentrations (170 ppm) than that of the Dawutang and Shimensi segments but close to the Xi'an W deposit (Fig. 2b and 8c). Tungsten mineralization occurs in Neoproterozoic strata in the Shiweidong segment, but these strata are lacking in the Dawutang and Shimensi segments. Therefore, recycled meteoric water may made variable contributions to the increased Sr concentration of ore-forming fluids.

Unlike the REEs in the D1 and D2 scheelite samples, the scheelite samples from the Xi'an deposit exhibited a depletion of MREEs and HREEs during the evolution of fluids (Fig. 6). The REE distribution pattern of the X1 scheelite samples from the Xi'an W deposit are similar to those from the Woxi W–Au–Sb deposit (Peng et al., 2005). The MREEs have the highest partition coefficient in scheelite; therefore, the crystallization of scheelite in a closed system would significantly deplete MREEs in the evolved fluids, whereas there would only be a slight variation in an open system (Li et al., 2018). The variation of the REE pattern of the samples from the Xi'an deposit was similar to that of the stage II scheelite samples from the Muguayuan W deposit, which suggests the precipitation of scheelite at a low water/mineral ratio.

Therefore, the evolution of the Xi'an deposit can help provide insight into the ore-forming fluids of the Dahutang deposit. The decomposition of plagioclase plays an important role in the evolution of the fluids. In different segments of the Dahutang deposit, recycled meteoric water makes variable contributions but for the W mineralization, the crystallization of hydrothermal minerals (particularly scheelite) controls the change in the composition of ore-forming fluids.

5.3. *Variation of oxygen fugacity of ore-forming fluids*

In nature, Eu has two valences: + 3 and + 2 (Henderson, 1984). There are three main factors that control the Eu anomalies in scheelite: (1) the Eu^{2+}/Eu^{3+} ratio in fluids, (2) the partition coefficient of Eu^{2+} and Eu^{3+} between scheelite and fluids, and (3) the Eu concentration of fluids (Shannon, 1976). The radius of the eightfold coordination of the Eu^{2+} ion is much larger than that of Ca^{2+}, which is not conducive to the replacement of Ca^{2+} in the scheelite crystal lattice by Eu^{2+} (Shannon, 1976). The radius of the eightfold coordination of Eu^{3+} is similar to the radius of other REE^{3+} ions, which is more compatible with Ca^{2+} replacement in the scheelite lattice. In addition, Eu^{3+} has a partition coefficient between scheelite and fluids that is similar to other REE^{3+}, but much higher than Eu^{2+} (Brugger et al., 2000b). Therefore, on a plot of chondrite-normalized Eu (Eu_N) versus Eu^*_N ($Eu^*_N = (Sm_N + Gd_N)/2$), the scheelite from Eu^{2+}-dominant reduced fluids plot parallel to the x-axis, whereas scheelite from Eu^{3+}-dominant oxidized fluids plot along a line with a slope of 1 (Ghaderi et al., 1999). The data for the D1 and D2 scheelite samples form a nearly horizontal line (Fig. 10), suggesting that Eu^{2+} is dominant in the ore-forming fluids of the Dahutang deposit. We note that the D2 samples from the Shiweidong segment show a trend with a slope near 1, suggesting that the $f(O_2)$ of the ore-forming fluids

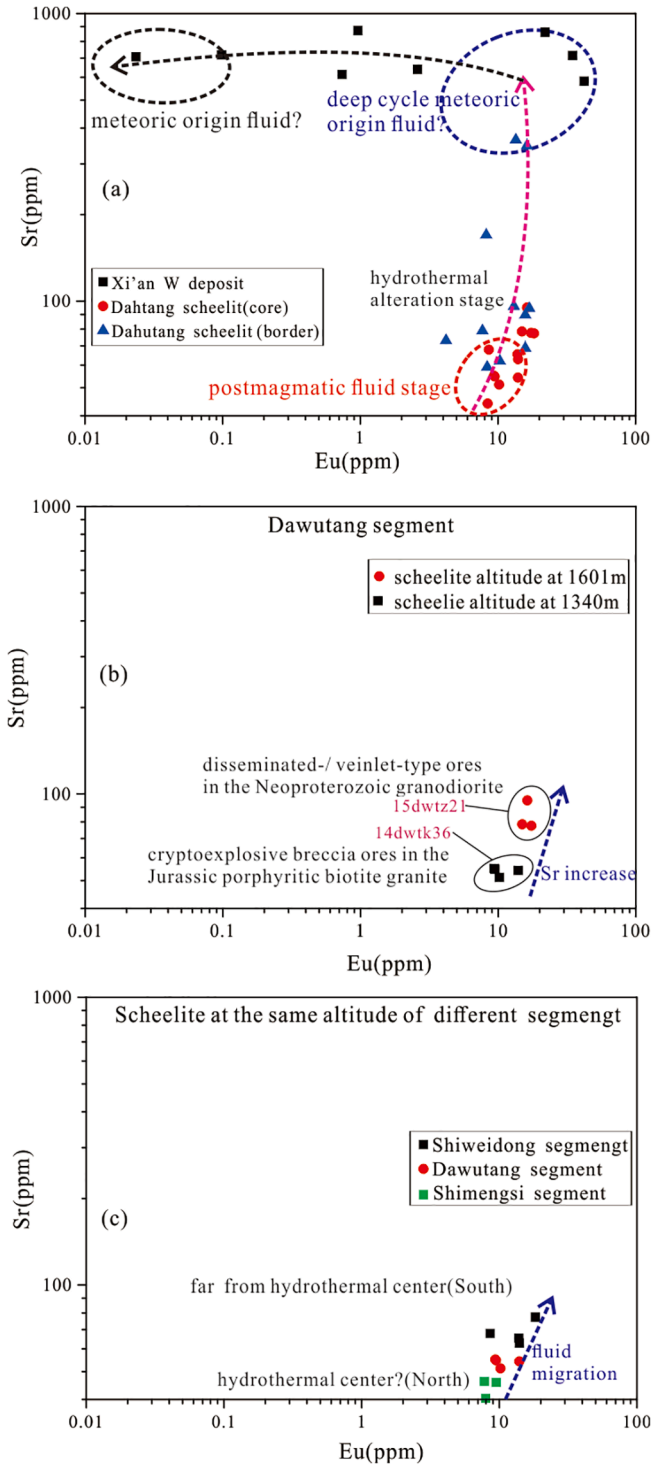

Fig. 8. Eu–Sr scatter plot of scheelite samples from the Dahutang tungsten deposit. (a) The Eu–Sr concentration of scheelite shows the evolution process of ore-forming fluid from the early magmatic hydrothermal solution, the altered hydrothermal solution after the alteration of surrounding rock, to the late mixing with the deep cycling of atmospheric original fluid. The evolution of the Sr concentration of scheelite during the late stage at the Dahutang deposit tends towards the scheelite from the deep cycling of atmospheric original fluid at the Xi'an deposit. (b) Scheelite in the same segment at the Dahutang deposit is characterized by an increasing Sr concentration with rising altitude. (c) Magma derived fluid of the Dahutang deposit may have experienced a process of migration from the north (Shimengsi) to the south and the replacement of the surrounding rock, and then mixing with the deep cycling of meteoric origin fluid in the Shiweidong segment (south). Shimengsi segment scheelite data are from Zhang et al. (2018a).

increased during fluid evolution up to the Shiweidong segment.

The oxygen fugacity of the tungsten ore-forming fluid strongly controls the migration and precipitation of tungsten from the fluid. Previous studies have shown a low $f(O_2)$ during early greisenization ($Log(fO_2) = -17.6$ to -17.8), which would allow wolframite and scheelite D1 to precipitate from the hydrothermal fluids. Oxygen fugacity increases during later greisenization with precipitation of scheelite D2, which would be unfavorable for wolframite deposition. At the same time, the crystallization of zinnwaldite (muscovite formed during greisenization) would lower the Fe concentration of hydrothermal fluids, which would further restrict the deposition of wolframite. Subsequently, the increasing fO_2 of the fluid inhibits the formation of wolframite or the decomposition of early wolframite (Liu and Ma, 1987a), whereas a higher $f(O_2)$ is beneficial to the formation of scheelite. A relatively high $f(O_2)$ and sufficient Ca concentration would cause the ore-forming fluid to begin scheelite precipitation. However, the ore-forming fluids would still be reduced, given the dominance of Eu^{2+} at the early greisenization stage. The reductive evolution of fluid to a low $f(O_2)$ is conducive to the formation of wolframite. With the addition of oxidized recycled meteoric water at the later greisenization and silicification stage, the fluids become more oxidized with Eu^{3+} dominant which would be conducive to the formation of scheelite D2.

The REE contents of the Xi'an scheelite samples vary greatly from the core to the rim, especially with respect to the fractionation of MREEs and HREEs; however, there was no δEu anomaly (Fig. 6a). The REE distribution curve of the X1 scheelite samples from the Xi'an W deposit is similar to that of samples from the Woxi W–Au–Sb deposit (Peng et al., 2005), which was formed by fluids with a high $f(O_2)$ (Gu et al., 2005; Peng et al., 2005). Hence, the fluid that formed the scheelite (core) of the Xi'an W deposit may be mainly Eu^{3+}, and the ore-forming fluids probably had a relatively high $f(O_2)$. The X2 scheelite samples also had no δEu anomaly, thus indicating that the fluids may be dominated by Eu^{3+} and have the same $f(O_2)$ (Fig. 9). On the plot of Eu^*_N versus Eu_N (Fig. 9), the data of the X1 and X2 scheelite samples from the Xi'an deposit plot as a line with a slope near 1, which indicated a Eu^{3+} dominant oxidized fluid; hence, the Xi'an W deposit was formed by oxidized fluids.

The chemical composition of veinlet-disseminated scheelite trace the ore-forming fluids of the Dahutang deposit were initially reduced and evolved to be oxidized. The ore-forming fluids of the Xi'an deposit were oxidized based on the chemical composition of scheelite. The increase in the oxygen fugacity of the ore-forming fluids of the Dahutang deposit led to the termination of wolframite crystallization and was favorable for

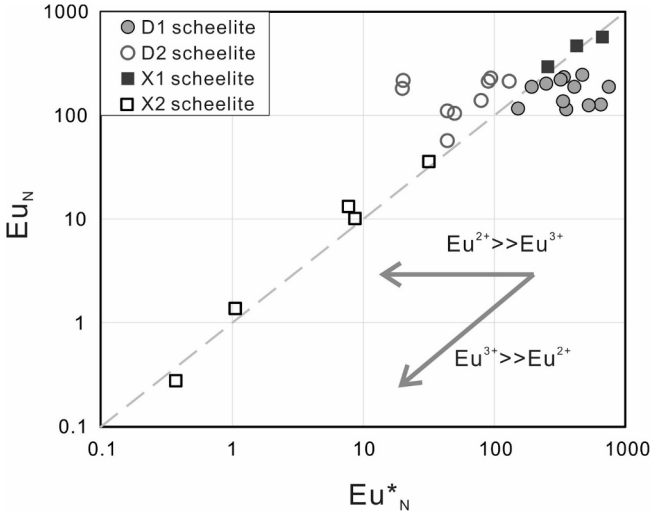

Fig. 9. Plot of chondrite-normalized Eu concentrations (Eu_N) vs. calculated Eu^*_N values of scheelite from the Dahutang and Xi'an deposits, where $Eu^*_N = (Sm_N + Gd_N)/2$. The dashed line represents 1:1 correlation line assuming that Eu_N is identical to Eu^*_N.

the precipitation of scheelite D2 to form the veinlet-disseminated W deposit.

6. Conclusions

(1) The mineralogy and in-situ trace element characteristics revealed that the W mineralization of the Dahutang deposit was formed in two stages. The early fluids were magma-derived with high Nb, Ta, and Mo concentrations, whereas the later fluids had lower Nb, Ta, and Mo concentrations. The early fluids contained low Eu and Sr concentrations, whereas the later fluids contained higher Eu and Sr concentrations. This implies that the decomposition of plagioclase in granodiorite played an important role in the precipitation of scheelite.
(2) The ore-forming fluids of the Xi'an W deposit were probably a mixture of metamorphic and meteoric water, which was characterized by the lowest Nb, Ta, and Mo concentrations but the highest Sr concentration of all scheelite samples.
(3) The ore-forming fluids at the early stage of the Dahutang deposit were reduced and evolved to oxidized to form the D2 scheelite, whereas the ore-forming fluids of the Xi'an deposit were oxidized. The increase in the $f(O_2)$ of the ore-forming fluids of the Dahutang deposit led to the termination of wolframite crystallization and was favorable for the precipitation of scheelite.

Declaration of Competing Interest

The authors declare that they have no known competing financial interests or personal relationships that could have appeared to influence the work reported in this paper.

Acknowledgements

This research is funded by the National Research and Development Program of China, China (2016YFC0600207, 2014CB440904) and National Natural Science Foundation of China, China (no. 42062006, 41962007) and China Geological Survey, China (no.12120114034501). We would like to thank Mr. Xinkui Xiang, Mr. Lanqing Liu and their coworkers from the Jiangxi Bureau of Geology, Mineral Resources, Exploration and Development, and the No. 916 Geological Team and Northwestern Geological Team for their field guidance and constructive discussions. Two reviewers and editors are much appreciated for their constructive comments. Engineers of the Nanjing FocuMS Technology Co. Ltd. are also grateful for their assistance with the in situ analysis of the scheelite.

References

Audétat, A., Pettke, T., 2003. The magmatic-hydrothermal evolution of two barren granites: A melt and fluid inclusion study of the Rito del Medio and Cañada Pinabete plutons in northern New Mexico (USA). Geochim. Cosmochim. Acta 67 (1), 97–121.
Biver, M., Shotyk, W., 2013. Stibiconite (Sb_3O_6OH), senarmontite (Sb_2O_3) and valentinite (Sb_2O_3): Dissolution rates at pH 2–11 and isoelectric points. Geochim. Cosmochim. Acta 109, 268–279.
Bottrell, S.H., Yardley, B.W.D., 1988. The composition of a primary granite-derived ore fluid from S.W. England, determined by fluid inclusion analysis. Geochim. Cosmochim. Acta 52 (2), 585–588.
Brugger, J., Bettiol, A.A., Costa, S., Lahaye, Y., Bateman, R., Lambert, D.D., Jamieson, D. N., 2000a. Mapping REE distribution in scheelite using luminescence. Mineral. Mag. 64 (5), 891–903.
Brugger, J., Etschmann, B., Pownceby, M., Liu, W., Grundler, P., Brewe, D., 2008. Oxidation state of europium in scheelite: Tracking fluid–rock interaction in gold deposits. Chem. Geol. 257 (1), 26–33.
Brugger, J., Lahaye, Y., Costa, S., Lambert, D., Bateman, R., 2000b. Inhomogeneous distribution of REE in scheelite and dynamics of Archaean hydrothermal systems (Mt. Charlotte and Drysdale gold deposits, Western Australia). Contrib. Miner. Petrol. 139 (3), 251–264.
Brugger, J.L., Etschmann, B., Chu, Y.S., Harland, C., Vogt, S., Ryan, C., Jones, H., 2006. The oxidation state of europium in hydrothermal scheelite: In situ measurement by Xanes spectroscopy. Can. Miner. 44 (5), 1079–1087.
Burnham CW. 1979. Magmas and hydrothermal fluids. In: In Geochemistry of Hydrothermal. pp, 71–136.
Carroll, M.R., Webster, J.D., 1994. Solubilities of sulfur, noble gases, nitrogen, chlorine, and fluorine in magmas. Rev. Mineral. Geochem. 30 (1), 231–279.
Cathles, L.M., 1990. Scales and effects of fluid flow in the upper crust. Science 248 (4953), 323–329.
Connolly, J.A.D., Thompson, A.B., 1989. Fluid and enthalpy production during regional metamorphism. Contrib. Miner. Petrol. 102 (3), 347–366.
Demicco, R.V., Lowenstein, T.K., Hardie, L.A., Spencer, R.J., 2005. Model of seawater composition for the Phanerozoic. Geology 33 (11), 877–880.
Ding, X., Jiang, S.Y., Ni, P., Gu, L.X., Jiang, Y.H., 2005. Zircon SIMS U-Pb geochronology of host granitoids in Wushan and Yongping copper deposits, Jiangxi Province. Geol. J. China Univ. 11 (3), 383–389 (in Chinese with English abstract).
Dolejš, D., Wagner, T., 2008. Thermodynamic modeling of non-ideal mineral–fluid equilibria in the system Si–Al–Fe–Mg–Ca–Na–K–H–O–Cl at elevated temperatures and pressures: Implications for hydrothermal mass transfer in granitic rocks. Geochim. Cosmochim. Acta 72 (2), 526–553.
Eugster, H.P., 1985. Granites and hydrothermal ore deposits: A geochemical framework. Miner. Mag. 49 (350), 7–23.
Feng, C.Y., Zhang, D.Q., Xiang, X.K., Li, D.X., Qu, H.Y., Liu, J.N., Xiao, Y., 2012. Re-Os isotopic dating of molybdenite from the Dahutang tungsten deposit in northwestern Jiangxi Province and its geological implication. Acta Geol. Sin. 28 (12), 3858–3868 (in Chinese with English abstract).
Ghaderi, M., Palin, J.M., Campbell, I.H., Sylvester, P.J., 1999. Rare earth element systematics in scheelite from hydrothermal gold deposits in the Kalgoorlie-Norseman region, Western Australia. Econ. Geol. 94 (3), 423–437.
Gleeson, S., Yardley, B., 2003. Surface-derived fluids in basement rocks: Inferences from palaeo-hydrothermal systems. J. Geochem. Explor. 78, 61–65.
Gleeson, S.A., Yardley, B.W.D., Munz, I.A., Boyce, A.J., 2003. Infiltration of basinal fluids into high-grade basement, South Norway: Sources and behaviour of waters and brines. Geofluids 3 (1), 33–48.
Gu, X.X., Liu, J.M., Schulz, O., Vavtar, F., Fu, S.H., 2005. REE geochemical evidence for the genesis of the Woxi Au-Sb-W deposit, Hunan Province. Geochemica. 34 (5), 428–442 (in Chinese with English abstract).
Han, Y., Zhang, C.H., Zhang, H., You, G.Q., Li, L.Y., 2016. Configuration of mid-neoproterozoic arc—Basin system in Eastern Jiangnan orogenic belt. Geol. Rev. 62 (2), 285–299 (in Chinese with English abstract).
Hanson, R.B., 1992. Effects of fluid production on fluid flow during regional and contact metamorphism. J. Metamorph. Geol. 10 (1), 87–97.
He, G.X., Zeng, D.B., 1987. Features and genesis of the Xi'an scheelite deposit, Taoyuan county, Hunan. Hunan Geol. 3, 23–29 (in Chinese with English abstract).
Henderson, P., 1984. Rare Earth Element Geochemistry. Elsevier, Amsterdam, pp. 1–501.
Holland, H.D., 1972. Granites, solutions, and base metal deposits. Econ. Geol. 67 (3), 281–301.
Hu, Z.H., Liu, D., Liu, S.B., Lang, X.H., Zhang, J.J., Chen, Y.C., Shi, G.H., Wang, Y.Y., Lei, T.H., Nei, L.M., Sha, M., Gong, L.X., Liu, Z.Q., 2015. Rock-forming and ore-forming ages and significance of Taqian Mo(W)deposit, Leping, Jiangxi, China. J. Chengdu Univ. Technol. 42 (3), 312–322 (in Chinese with English abstract).
Huang, L.C., Jiang, S.Y., 2014. Highly fractionated S-type granites from the giant Dahutang tungsten deposit in Jiangnan Orogen, Southeast China: Geochronology, petrogenesis and their relationship with W-mineralization. Lithos 202 (4), 207–226.
Jiang, S.Y., Peng, N.J., Huang, L.C., Xu, Y.M., Zhan, G.L., Dan, X.H., 2015. Geological characteristic and ore genesis of the giant tungsten deposits from the Dahutang ore-concentrated district in northern Jiangxi Province. Acta Petrol. Sin. 31 (3), 639–655 (in Chinese with English abstract).
Kerrick, D.M., Connolly, J.A.D., 1998. Subduction of ophicarbonates and recycling of CO2 and H2O. Geology 26 (4), 375–378.
Kuang, W.L., Gu, D.S., Liu, X.H., 2004. Discussion on the mineralization geological features and metallogenetic model of Woxi Au-Sb-W deposit in west Hunan. Gold. 25 (6), 10–15 (in Chinese with English abstract).
Li, X.-Y., Gao, J.-F., Zhang, R.-Q., Lu, J.-J., Chen, W.-H., Wu, J.-W., 2018. Origin of the Muguayuan veinlet-disseminated tungsten deposit, South China: Constraints from in-situ trace element analyses of scheelite. Ore Geol. Rev. 99, 180–194.
Li, X.H., Li, W.X., Li, Z.X., Lo, C.H., Wang, J., Ye, M.F., Yang, Y.H., 2009. Amalgamation between the Yangtze and Cathaysia Blocks in South China: Constraints from SHRIMP U-Pb zircon ages, geochemistry and Nd–Hf isotopes of the Shuangxiwu volcanic rocks. Precambr. Res. 174 (1), 117–128.
Li, X.H., Li, Z.X., Ge, W., Zhou, H., Li, W., Liu, Y., Wingate, M.T.D., 2003. Neoproterozoic granitoids in South China: Crustal melting above a mantle plume at ca 825 Ma? Precambr. Res. 122 (s 1–4), 45–83.
Li, Y., Pan, X.F., Zhao, M., Chen, G.H., Zhang, T.F., Liu, X., Zhang, C., 2014. LA-ICP-MS Zircon U-Pb Age, geochemical features and relations to the W-Cu mineralization of granitic porphyry in Zhuxi Skarn deposit, Jingdezhen, Jiangxi. Geol. Rev. 60 (3), 693–708 (in Chinese with English abstract).
Liu, J., Mao, J.W., Ye, H.S., Xie, G.Q., Yang, G.Q., Zhang, W., 2008a. Zircon LA-ICPMS U-Pb dating of Hukeng granite in Wugongshan area, Jiangxi Province and its geoehemical characteristics. Acta Petrol. Sin. 24 (8), 1813–1822 (in Chinese with English abstract).
Liu, Y., Deng, J., Li, ChaoFeng, Shi, GuangHai, Zheng, AiLi, 2007. REE composition in scheelite and scheelite Sm-Nd dating for the Xuebaoding W-Sn-Be deposit in Sichuan. Chin. Sci. Bull. 52 (18), 2543–2550.
Liu YJ, Cao LM. 1987. Introduction to Elemental Geochemistry. Beijing: Geologyical Publishing House, Beijing, 1–281 (in Chinese).
Liu, Y.J., Li, Z.L., Ma, D.S., 1982. The geochemical studies of tungsten bearing formation in South China. Sci. China Ser. B 12 (10), 939–950 (in Chinese with English abstract).

Liu YJ, Ma D-S. 1987a. Geochemistry of Tungsten. Beijing: Science Press, Beijing, 1–232 (in Chinese).
Liu, Y.J., Ma, D.S., 1987b. Geochemical characterisitcs of gold-bearing formation in south china. Contrib. Geol. Miner. Res. Res. 2 (4), 1–14 (in Chinese with English abstract).
Liu YJ, Sun CY, Ma DS. 1993. Metallogenic and Geochemical Background of Jiangnan-Type Gold Deposit. Nanjing University Press, Nanjing, 1–260 (in Chinese).
Liu, Y.S., Hu, Z.C., Gao, S., Günther, D., Xu, J., Gao, C.G., Chen, H.H., 2008b. In situ analysis of major and trace elements of anhydrous minerals by LA-ICP-MS without applying an internal standard. Chem. Geol. 257 (1), 34–43.
Liu, Z.G., Yu, J.M., Liu, S.Y., Zen, D.B., Lei, M.B., Ten, Y., 2000. REE characteristics of the Woxi Gold-Antimony-Tungsten deposit, Hunan Province. Miner. Deposits 19 (3), 270–278 (in Chinese with English abstract).
Lou, F.S., Shen, W.Z., Wang, D.Z., Shu, L.S., Wu, F.J., Zhang, F.R., Yu, J.H., 2005. Zircon U-Pb isotopic chronology of the Wugongshan dome compound Granite in Jiangxi Province. Acta Geol. Sin. 79 (5), 637–644 (in Chinese with English abstract).
Ma, D.S., Liu, Y.J., 1991. A study on geochemical characteristics and metallogenesis of stratabound gold deposit in Jiangnan metallogenic belt. Sci. China Ser. B 10, 424–433 (in Chinese with English abstract).
Ma, D.S., Liu, Y.J., 1992. Geochemical characteristics and genesis of stratabound gold deposits in Jiangnan gold metallogenic belt. Sci. China Ser. B 35 (2), 240–256.
Ma, L.F., Qiao, X.F., Ming, L.R., Fan, B.X., Ding, X.Z., 2002. Geological Atlas of China. Geological Publishing House, Beijing (in Chinese with English abstract).
MacRae, C.M., Wilson, N.C., Brugger, J., 2009. Quantitative cathodoluminescence mapping with application to a Kalgoorlie Scheelite. Microsc. Microanal. 15 (3), 222–230.
Mao, Z.-H., Liu, J.-J., Mao, J.-W., Deng, J., Zhang, F., Meng, X.-Y., Xiong, B.-K., Xiang, X.-K., Luo, X.-H., 2015. Geochronology and geochemistry of granitoids related to the giant Dahutang tungsten deposit, middle Yangtze River region, China: Implications for petrogenesis, geodynamic setting, and mineralization. Gondwana Res. 28 (2), 816–836.
Niu, H.C., Ma, D.S., 1992. Metallogenesis of stratabound gold deposits in West Hunan. Miner. Depsoits 11 (1), 65–75 (in Chinese with English abstract).
Peng, B., Frei, R., Xianglin, T., 2006. Nd-Sr-Pb isotopic geochemistry of scheelite from the Woxi W-Sb-Au deposit, Eastern Hunan: implicarions for sources and evolution of ore-forming fluids. Acta Geol. Sin. Engl. Ed. 80, 561–570.
Peng, J.T., Hu, R.Z., Zhao, J.H., Fu, Y.Z., Lin, Y.X., 2003. Scheelite Sm-Nd dating and quartz Ar-Ar dating for Woxi Au-Sb-W deposit, western Hunan. Chin. Sci. Bull. 48 (23), 2640–2646 (in Chinese with English abstract).
Peng, J.T., Hu, R.Z., Zhao, J.H., Fu, Y.Z., Yuan, S.D., 2005. Rare earth element (REE) geochemistry for scheelite from the Woxi Au–Sb–W deposit, western Hunan. Geochimica 34 (2), 115–122 (in Chinese with English abstract).
Peng, J.T., Zhang, D.L., Hu, R.Z., Wu, M.J., Liu, X.M., Qi, L., Yg, Y.u., 2010. Inhomogeneous distribution of rare earth elements (REEs) in scheelite from the Zhazixi W-Sb deposit, Western Hunan and its geological implications. Geol. Rev. 56 (6), 810–819 (in Chinese with English abstract).
Poulin, R.S., 2016. A Study of the Crystal Chemistry, Cathodoluminescence, Geochemistry and Oxygen Isotopes in Scheelite: Application Towards Discriminating among Differing Ore-Deposit Systems. Laurentian University, Sudbury, Ontario.
Poulin, R.S., Mcdonald, A.M., Kontak, D.J., Mcclenaghan, M.B., 2016. On the relationship between cathodoluminescence and the chemical composition of scheelite from geologically diverse ore-deposit environments. Can. Miner. 54 (5), 1147–1173.
Prowatke, S., Klemme, S., 2006. Trace element partitioning between apatite and silicate melts. Geochim. Cosmochim. Acta 70 (17), 4513–4527.
Raimbault, L., Baumer, A., Dubru, M., Benkerrou, C., Croze, V., Zahm, A., 1993. REE fractionation between scheelite and apatite in hydrothermal conditions. Am. Miner. 78 (11–12), 1275–1285.
Sciuba, M., Beaudoin, G., Grzela, D., Makvandi, S., 2019. Trace element composition of scheelite in orogenic gold deposits. Miner. Deposita.
Shannon, R.D., 1976. Revised effective ionic radii and systematic studies of interatomic distances in halides and chalcogenides. Acta Crystallogr. A 32 (5), 751–767.
Shi MK, Fu BQ, Jin XX, Zhou XC. 1993. Antimony Metallogeny in the Central Part of Hunan Province. Changsha: Hunan Press of Science and Technology. 1150. (in Chinese).
Shu, L.S., 2012. An analysis of principal features of tectonic evolution in South China Block. Geol. Bull. China 31 (7), 1035–1053 (in Chinese with English abstract).
Shu LS, Shi YS, Guo LZ. 1995. The Late Proterozoic Plate Tectonics and Collisional Kinematics in the Middle Part of the Jiangnan Belt. Nanjing: Nanjing University Publishing House, 1–174. (in Chinese with English abstract).
Shu, L.S., Sun, Y., Li, Y.J., 1993. Paleomagnetism features and its tectonic significance in the middle part of the Jiangnan balt, south China. J. Nanjing Univ. Natl. Sci. 1, 14 (in Chinese with English abstract).
Song, G., Qin, K., Li, G., Evans, N.J., Chen, L., 2014. Scheelite elemental and isotopic signatures: Implications for the genesis of skarn-type W-Mo deposits in the Chizhou Area, Anhui Province, Eastern China. Am. Miner. 99 (2-3), 303–317.
Song, W.-L., Yao, J.-M., Chen, H.-Y., Sun, W.-D., Ding, J.-Y., Xiang, X.-K., Zuo, Q.-S., Lai, C.-K., 2018. Mineral paragenesis, fluid inclusions, H-O isotopes and ore-forming processes of the giant Dahutang W–Cu–Mo deposit, South China. Ore Geol. Rev. 99, 116–150.
Sun, K., Chen, B., 2017. Trace elements and Sr-Nd isotopes of scheelite: Implications for the W-Cu-Mo polymetallic mineralization of the Shimensi deposit, South China. Am. Miner. 102 (5), 1114–1128.
Sylvester, P.J., Ghaderi, M., 1997. Trace element analysis of scheelite by excimer laser ablation-inductively coupled plasma-mass spectrometry (ELA-ICP-MS) using a synthetic silicate glass standard. Chem. Geol. 141 (1), 49–65.
Ten, Y., Liu, Z.G., Yu, J.M., Zen, D.B., Tan, B.F., 1999. REE geochemical features of Woxi Au-Sb-W deposit in Western Hunan. J. Guilin Inst. Technol. 19 (2), 108–113 (in Chinese with English abstract).
Van Daele, J., Hulsbosch, N., Dewaele, S., Boiron, M.C., Piessens, K., Boyce, A., Muchez, P., 2018. Mixing of magmatic-hydrothermal and metamorphic fluids and the origin of peribatholitic Sn vein-type deposits in Rwanda. Ore Geol. Rev. 101, 481–501.
Wan, J.M., 1985. Fluid inclusions and light stable isotopes of scheelite in Xi'an deposits, Western Hunan. Geogeochem. 9, 67 (in Chinese with English abstract).
Wan, J.M., 1986. Rare earth element geochemical study of the Xi'an tungsten deposit, West Hunan. Geochemica. 2, 183–192 (in Chinese with English abstract).
Wang, X.-L., Zhao, G., Zhou, J.-C., Liu, Y., Hu, J., 2008. Geochronology and Hf isotopes of zircon from volcanic rocks of the Shuangqiaoshan Group, South China: Implications for the Neoproterozoic tectonic evolution of the eastern Jiangnan orogen. Gondwana Res. 14 (3), 355–367.
Watson, E.B., Baxter, E.F., 2007. Diffusion in solid-earth systems. Earth Planet. Sci. Lett. 253 (3), 307–327.
Wilson, N., Webster-Brown, J., Brown, K., 2007. Controls on stibnite precipitation at two New Zealand geothermal power stations. Geothermics. 36 (4), 330–347.
Wing, B.A., Ferry, J.M., 2002. Three-dimensional geometry of metamorphic fluid flow during Barrovian regional metamorphism from an inversion of combined petrologic and stable isotopic data. Geology 30 (7), 639–642.
Xiang, X.K., Wang, P., Sun, D.M., Zhong, B., 2013a. Re-Os isotopic age of molybdeinte from the Shimensi tungsten polymetallic deposit in northern Jiangxi province and its geological implications. Geol. Bull. China 32 (11), 1824–1831 (in Chinese with English abstract).
Xiang, X.K., Wang, P., Zhan, G.N., Sun, D.M., Zhong, B., Qian, Z.Y., Tan, R., 2013b. Geological characteristics of Shimensi tungsten polymetallic deposit in northern Jiangxi Province. Miner. Deposits 32 (6), 1171–1187 (in Chinese with English abstract).
Yang, C.P., Xia, F., Pan, J.Y., Zhang, Y., Liu, G.Q., 2014. Single-zircon LA-ICP-MS U-Pb dating and their implications of the Granite in the Lianhuaxin Copper Molybdenum polymetallic deposit, Xiushui County, Jiangxi Province. J. East China Inst. Technol. 37 (2), 192r198 (in Chinese with English abstract).
Zhang, D.L., Peng, J.T., 2012. Rare-earth element geochemistry in Ca-bearing minerals from the Xianghuapu tungsten deposit, Hunan Province, China. Acta Petrol. Sin. 28 (1), 65–74 (in Chinese with English abstract).
Zhang, L.G., 1985. Stable isotope geological study on W-Sb-Au deposit in upwarped district, Xuefengshan, Westen Hunan. Geol. Prospect. 21 (11), 31–34 (in Chinese with English abstract).
Zhang, L.L., 2013. The Genetic Relationship between the Geochemical Characteristics of Granites and Mineralization in Suoyidong Mine of the Tungsten Ore Field of Dahutang in Jiangxi Province, South China. East China University of Technology, Nanchang (in Chinese with English abstract).
Zhang, M.Y., Feng, C.Y., Li, D.X., Wang, H., Zhou, J.H., Ye, S.Z., Wang, G.H., 2016. Geochronological study of the Kunshan W-Mo-Cu deposit in the Dahutang area, northern Jiangxi Province and its geological significance. Geotectonica Et Metallogenia. 40 (3), 503–516 (in Chinese with English abstract).
Zhang, Q., Zhang, R.Q., Gao, J.F., Lu, J.J., Wu, J.W., 2018a. In-situ LA-ICP-MS trace elemental analyses of scheelite and wolframite: Constraints on the genesis of veinlet-disseminated and vein-type tungsten deposits, South China. Ore Geol. Rev. 99, 166–179.
Zhang, Y., Pan, J.Y., Ma, D.S., Dan, X.H., Zhang, L.L., Xu, G.H., Yang, C.P., Jiang, Q.X., Jiang, C.Q., 2017. Re-Os Molybdenite age of Dawutang tungsten ore district of northwest Jiangxi and its geological significance. Miner. Deposits 36 (3), 749–769.
Zhang Y. 2018. Ore-Forming Fluid Evolution and Sb-Au-W Metallogenesis in the Central Hunan-Northwestern Jiangxi, South China. Nanjing: Najing University, 1-116 (in Chinese with English abstract).
Zhang, Y., Gao, J.-F., Ma, D.-S., Pan, J., 2018b. The role of hydrothermal alteration in tungsten mineralization at the Dahutang tungsten deposit, South China. Ore Geol. Rev. 95, 1008–1027.
Zhang Y, Liu NQ, Pan JY, Xiang XK, Jiang QX, Jiang CQ, Jiang YY, Ding WK. 2018c. The Superposition of Alkaline by Acidic Hydrothermal Alteration and Its Formation Mechanism at Dahutang Tungsten Deposit, South China. Science Press, Beijing, 1–145 (in Chinese with English abstract).
Zhang, Y., Ma, D.S., Pan, J.Y., Wu, H., Chen, F.N., 2018d. W-Au-Sb differentiation mineralization and crustal-scale fluid evolution in the Xiangzhong basin, Low temperature metallogenic belt, south China. Contrib. Geol. Miner. Res. Res. 33 (3), 319–334 (in Chinese with English abstract).
Zhang, Y.Z., Wang, Y.J., Geng, H.Y., Zhang, Y.H., Fan, W.M., Zhong, H., 2013. Early Neoproterozoic (~850Ma) back-arc basin in the Central Jiangnan Orogen (Eastern South China): Geochronological and petrogenetic constraints from meta-basalts. Precambr. Res. 231 (Supplement C), 325–342.
Zhao, W.W., Zhou, M.-F., Williams-Jones, A.E., Zhao, Z., 2018. Constraints on the uptake of REE by scheelite in the Baoshan tungsten skarn deposit, South China. Chem. Geol. 477, 123–136.
Zhong YF, Ma CQ, She ZB, Lin GC, Xu HJ, Wang RJ, Yang KG, Liu Q. 2005. SHRIMP U-Pb Zircon Geochronology of the Jiuling Granitic Complex Batholith in Jiangxi Province. 30(6), 685–691 (in Chinese with English abstract).